7. LANDSLIDE HAZARD ASSESSMENT

Nothing is more dangerous
than underestimating a hazard.

There are many good reasons
not to avoid hazards.

A hazard is the likelihood that a danger will materialize. A natural hazard is the hazard posed by a potentially damaging natural event or process, such as an earthquake, flood, volcanic eruption, snow avalanche, hurricane, ground subsidence or mass movement. Landslide hazard refers to the potential for the occurrence of a damaging slope failure within a given area and in a given period. To properly define landslide hazard, the magnitude, size, or dimension of the expected failure must also be quantified, deterministically or in probabilistic terms, because the "magnitude" of the event is linked to its destructive power. Landslide hazard is portrayed on maps. A landslide hazard map partitions a territory based upon different levels of landslide hazard (landslide hazard zoning). As it will become clear later, producing a single landslide hazard map is problematic, as different hazard conditions (or probabilities) must be shown on the same map. An ensemble of maps can be prepared to show landslide hazard, and displayed in a GIS.

In this chapter, I first examine a definition of landslide hazard, I then introduce a probabilistic model for landslide hazard assessment that fulfils the adopted definition, and I discuss known problems with the given definition and limitations of the proposed probability model. Next, I show three examples of the application of the proposed probability model for different types of landslides and at different scales, from the catchment to the national scale. In the first example, I illustrate an attempt to determine landslide hazard in the Staffora River basin (§ 2.6), exploiting a detailed multi-temporal inventory map and thematic information on geo-environmental factors associated with landslides. In the second example, I describe an attempt to determine levels of landslide hazard in Italy, based on synoptic information on geology, soil types and morphology, and an archive inventory of historical landslide events. In the third example, I exploit a physically-based computer model capable to simulating rock falls for the determination of rock fall hazard in south-eastern Umbria (§ 2.5).

7.1. Background and definitions

Physical scientists define a natural hazard either as the probability that a reasonably stable condition may change abruptly (Scheidegger, 1994), or as the probability of occurrence of a potentially damaging phenomenon within a given area and in a given period of time (Varnes and the IAEG Commission on Landslides and other Mass-Movements, 1984). Vandine *et al*.

(2004) define landslide hazard the estimate of the probability of occurrence of a specific landslide and that the landslide being a threat to an element at risk, without considering the effects or potential consequences.

The definition proposed by Varnes and the IAEG Commission on Landslides and other Mass-Movements, (1984) remains the most widely accepted definition for natural hazard and for maps portraying its distribution over a region (IDNHR, 1987; Starosolszky and Melder, 1989; Horlick-Jones *et al.*, 1995; Murck *et al.*, 1997). The definition incorporates – more or less explicitly – the concepts of: (i) magnitude, (ii) geographical location, and (iii) time recurrence. The first refers to the "size" or "intensity" of the natural phenomenon which conditions its behaviour and destructive power. The second implies the ability to identify the place "where" the phenomenon will occur or may develop. The third refers to the temporal frequency of the event, i.e., the ability to predict "when" or how frequently the expected event will happen (Guzzetti *et al*., 1999a).

Application of the given definition to the various natural hazards differs, making conceptual and practical comparison and integration of hazard assessments difficult, if not impossible (Guzzetti *et al.*, 1999a; Natural Hazard Working Group, 2005). Without the ambition of completeness, I now examine differences in the assessment of the hazard for some of the most common natural hazards, namely: earthquakes, floods, volcanic eruptions and mass movements. Traditionally, earthquake predictive models attempt to define hazard in terms of magnitude – a quantitative measure of the energy released by a seismic event –, affected area, and time recurrence. Ideally, earthquake hazard assessments largely fulfil the definition of hazard previously mentioned. Unfortunately, scientists are generally unable to predict at the same time and with the required accuracy where and when an earthquake will take place, and how severe it will be. Amongst scientists there is a general consensus that with the present state of knowledge the exact (or even approximate) time of an earthquake cannot be predicted. Probabilistic Seismic Hazard Analysis is based on the statistical analysis of past earthquake events. Despite some criticism, PSHA remains the most widely applied method to define seismic risk (Castaños and Lomnitz, 2002; Bommer, 2003; Wang *et al*., 2003).

Despite the different meanings of the term "flood" (Baker, 1994), flood hazard evaluation essentially consists in the temporal prediction of an extreme hydrological event of a given magnitude (i.e., peak water flow or volume), whereas geographical location and spatial extent of the potentially inundated areas are determined from other sources of information, such as historical records and ground morphology. Estimates of the temporal occurrence of floods are mainly obtained from probabilistic analysis of the historical records of water levels or discharge measurements. For many gauging stations the record of measurements is short, and extrapolation techniques are used to obtain estimates of flood levels or water discharge for longer periods. Extrapolation inevitably introduces uncertainty in the hazard assessment. Where catchments are small, establishing hazard from water flow measurements may not be adequate (lack of warning time), or measurements may be completely lacking ("ungauged" basins). In these areas, the temporal prediction of an extreme hydrological event is obtained by studying measured, estimated, or forecasted rainfall. This undoubtedly introduces uncertainties in the hazard assessment. The extent and location of the potentially inundated areas are obtained from historical information and through the application of conceptual (simplified), physically based flood models, assuming a detailed description of topography and an input hydrograph. Accuracy of DTM and significance of the selected hydrograph are fundamental for the quality and relevance of flood spatial hazard assessments.

For volcanoes, the area affected by the eruption is implicitly defined in the analysis, i.e., the same volcano, which is usually well known in space. Before or during an eruption, scenarios are prepared to predict where individual or multiple lava flows or pyroclastic flows can travel and at what speed. The areas potentially affected by ash falls can also be determined. Again, these models (mostly physically based) are determined from external sources of information. The temporal occurrence of an eruption is estimated assimilating geological and volcanological knowledge, historical information and – most importantly – monitoring of physical and chemical properties, at depth and on the surface, including topographic deformations. The magnitude and destructiveness of an eruption depend largely on the type of the volcano. It is established mostly heuristically through the analysis of past eruptions and the recent behaviour of the investigated volcano.

For mass movements a conceptual confusion arises from the use of the same term "landslide" to address both the landslide deposit (the failed mass) and the movement of slope material or of an existing landslide mass (Bosi, 1978; Cruden, 1991; Guzzetti *et al*., 1999a). It is like mistaking an earthquake with its ground effects, an eruption with the area affected by lava flows or ash falls, or a river flood with the inundated area. Landslide predictive models most commonly attempt to identify only "where" landslides may occur over a given region on the basis of a set of relevant environmental characteristics. Such models do not directly incorporate "time" and "magnitude", i.e., size (Fell, 1994; Cardinali *et al*., 2002, Reichenbach *et al*., 2005), speed (Cruden and Varnes, 1996), kinetic energy (Hsu, 1975; Sassa, 1988), destructiveness (Hungr, 1997) or momentum of the failed mass. For this reason, these models cannot be correctly defined as hazard models (§ 6). Predictive models of landslide movement are generally confined to single slopes or individual small catchments (e.g., in the case of debris flows) where detailed geotechnical site investigations attempt to assess when and to what extent the slope-forming material, frequently an existing landslide deposit, will move. Also in this case the term hazard is somewhat incorrect since the location of the phenomenon under study is implicit, or derives from information acquired from other sources.

The wide spectrum of landslide phenomena (Figure 1.1) and the complexity and variability of their interactions with the environment, both natural and human, make the acceptance of a single definition of landslide hazard difficult. For example, very large and fast moving rock avalanches are the most destructive and hazardous mass movements, but are relatively rare events. Slow-moving, deep-seated failures rarely claim lives but can cause large property damage. Fast-moving soil slips and debris flows cause widespread damage and casualties, and are as frequent as their potential triggers (i.e., high intensity rainfall events). Rock falls, despite their often small size, are among the most destructive mass movements, and a primary cause of landslide fatalities in many areas. Each type of slope movement poses different threats and may require a separate assessment, based on distinct definitions of landslide hazard.

Recurrence, the expected time for the repetition of an event, is evaluated studying historical records (§ 3.3.1, § 4.5) or multiple-temporal inventories (§ 3.3.4). Historical data are difficult to obtain for single landslides or landslide prone areas. Despite the lack of consensus on the reliability and usefulness of historic information, where historical information is available it can be used for the temporal evaluation of landslide hazard at various scales (Guzzetti *et al*., 1994; 2003; Ibsen and Brunsden, 1996; Cruden, 1997; Evans, 1997; Glade, 1998). Historical records may be integrated with temporal data derived from dendrocronology and other dating techniques which have been used by some investigators to date landslide deposits (Stout, 1977; DeGraff and Agard, 1984; Trustrum and De Rose, 1988; Fantucci and Sorriso-Valvo,

1999; Lang *et al*., 1999; Stefanini, 2004). For first-time failures (Hutchinson, 1988) recurrence is not applicable. First-time landslides occur at or close to peak strength values, whereas reactivations occur between peak and residual conditions. Thus, first-time landslides provide little information on the behaviour of reactivations. Additionally, each time a landslide occurs, the topographic, geological and hydrological settings of the slope change, often dramatically, giving rise to different conditions of instability (§ 6.3.1). These changes allow geomorphologists to identify landslides and understand mechanisms and causes of failures, but limit their ability to forecast new landslides of reactivations.

Finally, quantitative landslide hazard models predict the occurrence of future slope failures under the general assumption that in any given area slope failures will occur in the future under the same circumstances and because of the same conditions that caused them in the past. I examined the problems encountered in adopting the principle that "the past is the key to the future" when I introduced rationale for landslide mapping (§ 3.1) and when I discussed landslide susceptibility assessment (§ 6.2.1, § 6.3.1). The same arguments apply to landslide hazard evaluation.

7.2. Probabilistic model for landslide hazard assessment

In their well-known report, Varnes and the IAEG Commission on Landslides and other Mass-Movements (1984) proposed that the definition adopted by UNDRO for all natural hazards be applied to mass movements. Landslide hazard is therefore "the probability of occurrence within a specified period of time and within a given area of a potentially damaging phenomenon". Guzzetti *et al.* (1999a) amended the definition to include the magnitude of the event. Hence, the definition becomes:

Landslide hazard is the probability of occurrence within a specified period and within a given area of a landslide of a given magnitude. (7.1)

For a landslide hazard forecast, the area and period for the prediction are simple to decide (albeit difficult to know). Definition of magnitude is more difficult because, in contrast to other natural hazards (e.g., earthquakes, volcanic eruptions, hurricanes), no unique measure of landslide magnitude is available. For earthquakes, magnitude is a measure of the energy released during an event ranked by the well known Richter scale, developed by Charles Richter and Beno Gutenberg. For volcanic eruptions, the Volcanic Explosivity Index devised by Christopher G. Newhall and Steve Self provides a relative measure (in 8 grades) of the explosiveness of eruptions based on a number of things that can be observed during an eruption. For hurricanes, the Saffir-Simpson scale measures the intensity of a hurricane in 5 grades, based on wind speed and atmospheric pressure, and gives an estimate of the potential property damage and flooding expected from a hurricane landfall. For landslides a measure of the energy released during failure is difficult to obtain. Malamud *et al*. (2004a) introduced a landslide-event magnitude scale, based on the number of landslides triggered by a meteorological or seismic event. Hungr (1997) proposed destructiveness to be a measure of landslide magnitude. Raetzo *et al*. (2001) introduced an intensity scale for the magnitude of the damage. Building on the latter definitions, Cardinali *et al.* (2002), Guzzetti (2004) and Reichenbach *et al.* (2005) defined landslide destructiveness as a function of the landslide volume and of the expected landslide velocity, the latter obtained from the landslide type. For large regions, landslide volume and velocity are difficult to evaluate systematically, making the approach impracticable. Alternatively, where slope failures are chiefly slow moving slides

and slide earth-flows, destructiveness can be related to the area of the landslide, information which is readily available from landslide inventory maps.

The definition of landslide hazard given in proposition 7.1 incorporates the concepts of location, time and size. To complete a hazard assessment one has to predict "where" a landslide will occur, "when", or how frequently it will occur, and "how large" the landslide will be. In mathematical terms, this can be written as:

$$H_L = P[A_L \geq a_L \text{ in a time interval } t, \text{ given } \{\text{morphology, lithology, structure, land use, ...}\}] \quad (7.2)$$

where, A_L is the landslide area, measured e.g., in square meters. For any given area, equation 7.2 expresses landslide hazard as the conditional probability of landslide size, $P(A_L)$, of landslide occurrence in an established period, $P(N_L)$, and of landslide spatial occurrence, S, given the local environmental setting. Assuming independence among the three probabilities, the landslide hazard, i.e., the joint probability is:

$$H_L = P(A_L) \times P(N_L) \times S \quad (7.3)$$

In the previous chapters, I have shown how to obtain the three probabilities in equation 7.3. The probability of landslide size can be estimated from the analysis of the frequency-area distribution of known landslides (§ 5, and equations 5.3 and 5.4). The probability of landslide occurrence in an established period can be estimated from the analysis of archive or multi-temporal inventories, and can be quantified adopting a Poisson or a binomial distribution model for the occurrence of the landslide events (§ 4.5, and equations 4.7 and 4.8). Susceptibility, the spatial probability of landslide occurrence, can be obtained using a variety of methods and techniques (§ 6.2). For probabilistic landslide hazard assessments, susceptibility must be obtained with indirect, quantitative methods that provide numerical (probabilistic) estimates of the spatial probability of landslide occurrence (§ 6.2.3).

The proposed probability model for landslide hazard relays on the same assumptions on which landslide mapping (§ 3.1) and the three considered individual probability models are based (see § 4.5, § 5.2, § 6.2.1). Failures to comply with one or all of the assumptions will affect the reliability of the model and the relevance and applicability of the results. In § 7.3.5 I will investigate the problems posed by each of the assumptions, including examples of how to evaluate their impact on a landslide hazard assessment. In addition, independence between the three probabilities is assumed. From a geomorphological point of view, this assumption is strong and may not hold, always and everywhere. In many areas one may expect slope failures to be more frequent (time component) where landslides are more abundant and landslide area is large (spatial component). However, given the lack of understanding of landslide phenomena, independence is an acceptable first approximation that makes the problem mathematically tractable (Guzzetti *et al.*, 2005a). The assumption of independence is a simplification, and more complex models can be constructed using, e.g., Bayesian reasoning or Copulae. However, these approaches require the investigator to know the marginal probabilities. This is rather difficult, given the general lack of information on the statistics of landslide size and on the temporal statistics of slope failures.

7.3. Landslide hazard model for the Staffora River basin

In this section, I discuss a landslide hazard assessment prepared for the Staffora River basin, in Lombardy Region. The hazard assessment was obtained by exploiting the thematic and landslide information available for the study area and presented in § 2.6, and it relies on the probabilistic landslide hazard model introduced in section § 7.2.

To ascertain landslide hazard, the territory of the Staffora River basin – which extends for 275 km^2 – was partitioned into 2243 homogenous mapping units. For the purpose, the same procedure used to partition the Upper Tiber River basin for landslide susceptibility assessment (§ 6.4) was adopted. Starting from a DEM with a ground resolution of 20 m × 20 m, and a geographically coherent simplified representation of the main drainage lines, the territory was first subdivided into slope units (§ 6.2.2). The slope units were then further subdivided according to the main rock types cropping out in the basin. The further partitioning, solved problems of slope units characterized by rock types with different landslide abundance (i.e., different susceptibility). In this way, the study area was subdivided into 2243 geo-hydrological units, which represent the mapping units used for the hazard assessment.

Most of the landslide information needed to ascertain landslide hazard was obtained from the detailed multi-temporal landslide inventory map presented in § 2.6, which shows 3922 landslides, including 89 very old, relict mass movements. Figure 7.1 shows the multi-temporal landslide inventory used for the analysis, and Table 7.1 summarizes statistics of the mapped landslides, for different periods. In the following, I will exploit the temporal information on landslides shown in the multi-temporal inventory to determine the temporal probability of slope failure occurrence, and to verify the performance of the obtained landslide susceptibility model.

Table 7.1 – Staffora River basin. Landslide descriptive statistics obtained from the available multi-temporal inventory map shown in Figure 7.1. Percentage of landslide area (*) computed with respect to the total area covered by landslides (A_0–E_2).

		LANDSLIDES	*LANDSLIDE AREA*	
INVENTORY	*ESTIMATED LANDSLIDE AGE*	Number	Total	Percentage*
		#	km^2	%
A_0	very old (relict)	89	34.72	49.30
A_1	older than 1955	1443	38.24	54.30
A_2	1955 active	306	2.46	3.49
B_1	1955-1975	318	2.38	3.39
B_2	1975 active	685	4.41	6.26
C_1	1975-1980	89	1.32	1.87
C_2	1980 active	305	2.40	3.41
D_1	1980-1994	455	2.06	2.92
D_2	1994 active	175	1.36	1.94
E_1	1994-1999	19	0.65	0.93
E_2	1999 active	38	0.85	1.21
A_0–A_1	very old and older than 1955	1532	63.22	90
A_0–E_2	very old to 1999 active	3922	70.42	100
A_1–E_2	older than 1955 to 1999 active	3833	46.43	66
A_2–E_2	1955 active to 1999 active	2390	12.08	17

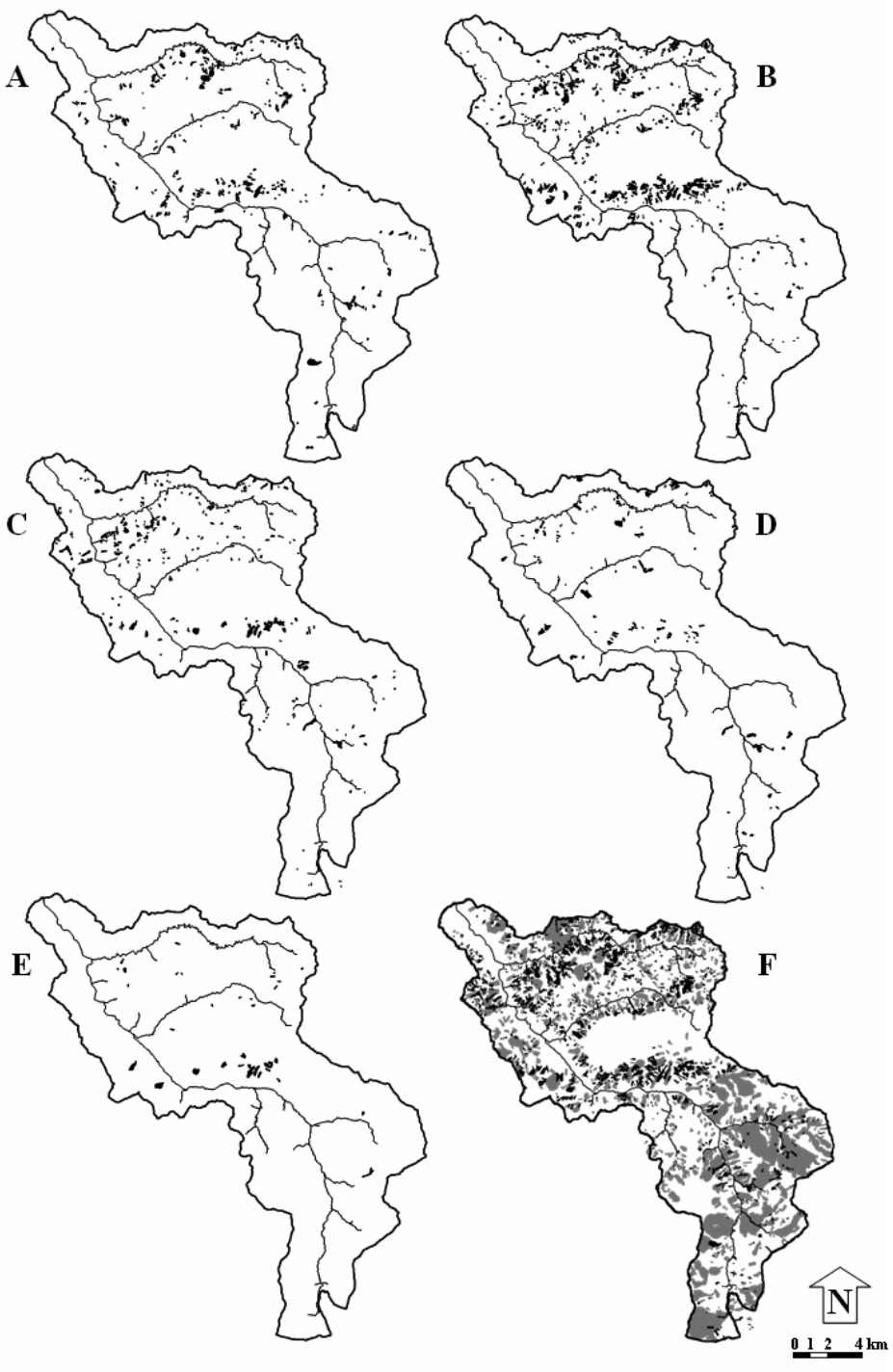

Figure 7.1 – Staffora River basin. Multi-temporal landslide inventory map used to ascertain landslide hazard. Landslide inventory prepared through the interpretation of five sets of aerial photographs of different dates (§ 2.6). Capital letters indicate the year of the aerial photographs used to compile the inventory. F shows the entire multi-temporal inventory map, which includes relict and old slides (shown in grey) identified in the 1955 aerial photographs. Characteristics of aerial photographs are: A; 18 July 1955, black and white, 1:33,000 scale. B; winter 1975, black and white, 1:15,000. C; summer 1980, colour, 1:22 000. D; summer 1994, black and white, 1:25,000. E; 22 June 1999, colour, 1:40,000.

7.3.1. Probability of landslide size

To ascertain the probability of landslide size (a proxy for landslide magnitude), I selected the multi-temporal inventory map covering the 45-year period from 1955 to 1999. This inventory consists of 2390 landslides (A_2–E_2 in Table 7.1). The area of the individual landslides in the inventory was obtained from the GIS. Care was taken to calculate the exact size of the landslide, avoiding topological and graphical problems related to the presence of smaller landslides inside larger mass movements. For convenience, the crown area and the deposit were merged together, and the total landslide area was used in the analysis. Old and relict mass movements were excluded from the analysis and only recent and active landslides were used.

Figure 7.2.A shows the probability density of landslide area in the Staffora River basin. Two estimates of the probability density are shown. I obtained the first estimate (blue solid line) using the inverse Gamma distribution of Malamud *et al.* (2004a) (eq. 5.4), and I obtained the second estimate (red dotted line) using the double-Pareto distribution of Stark and Hovius (2001) (eq. 5.3).

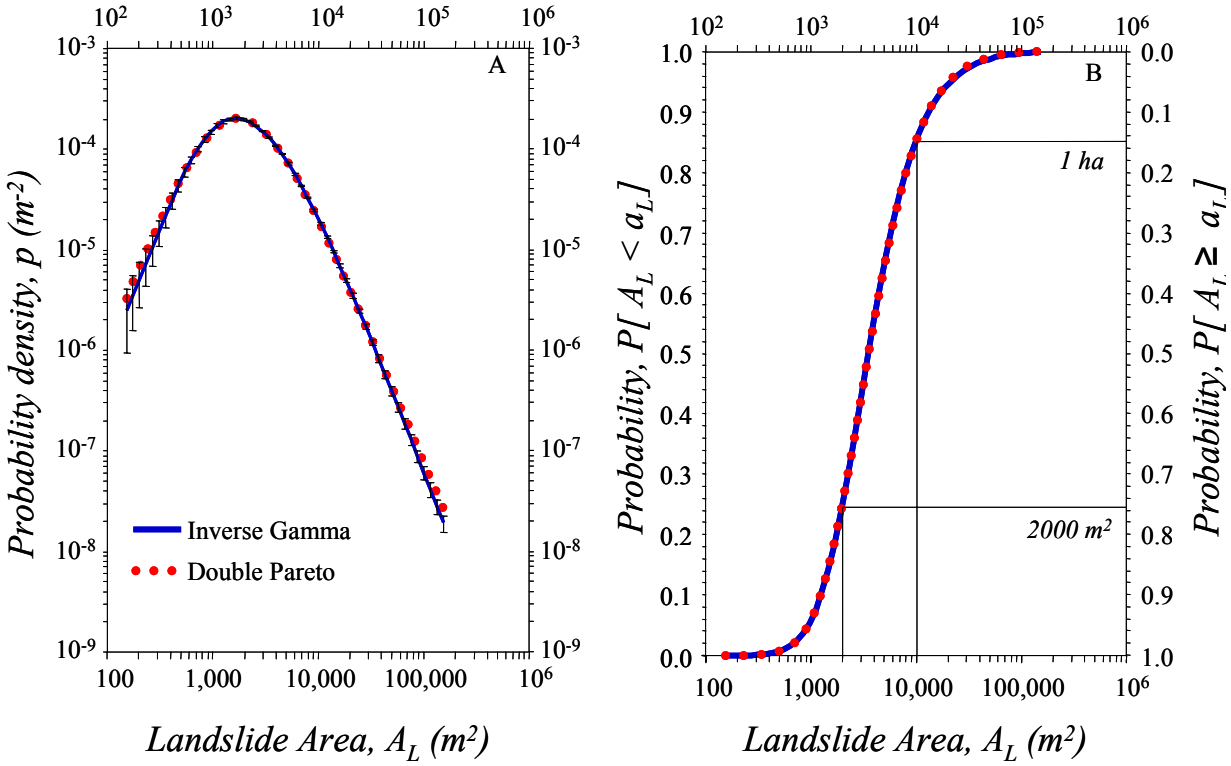

Figure 7.2 – Probability density (A) and probability (B) of landslide area in the Staffora River basin. Solid blue line is inverse gamma distribution (Malamud *et al.*, 2004). Dotted red line is a double Pareto distribution (Stark and Hovius, 2001). Error bars in A indicate the range between the 5th and the 95th percentiles for the truncated inverse Gamma function.

With the available landslide dataset, the two probability distributions provide very similar results and differ slightly only in the slope of the tails of the distributions (for inverse Gamma, $\alpha+1 = 2.77$, std. dev. = 0.08, for double Pareto, $\alpha+1 = 2.50$, std. dev. = 0.05). Figure 7.2.B shows the probability that a landslide will have an area smaller than a given size (left axis), or the probability that a landslide will have an area that exceeds a given size (right axis). Figure

7.2.B also shows the probability that a landslide in the Staffora River basin exceeds an area of 2000 m^2 and an area of one hectare, which are found to be 0.75 and 0.15, respectively. These values will be used to ascertain landslide hazards (Figure 7.7).

7.3.2. Probability of temporal landslide occurrence

To ascertain the temporal probability of landslide occurrence I selected the same multi-temporal inventory map covering the 45-year period from 1955 to 1999, i.e., A_2–E_2 in Table 7.1. First, the number of landslide events in each mapping unit was counted in the GIS, and the average rate of landslide events was established. Next, based on the past rate of landslide occurrence, landslide recurrence (i.e., the expected time between successive failures) was obtained for each mapping unit. Lastly, knowing the mean recurrence interval of landslides in each mapping unit (from 1955 to 1999), assuming the rate of failures will remain the same for the future, and adopting a Poisson probability model (eq. 4.7), the exceedance probability of having one or more landslides in each mapping unit was computed.

Figure 7.3 shows the landslide temporal exceedance probability for different periods, from 5 to 50 years. As expected, the probability of having one or more slope failure increases with time. Based on the historical record of landslides obtained from the multi-temporal inventory map, after 50 years many slopes in the Staffora River basin have a high to very probability of experiencing mass movements.

7.3.3. Spatial probability of landslides

I obtained landslide susceptibility for the Staffora River through discriminant analysis of 46 thematic variables, including morphology (24 variables derived from a 20 m × 20 m DEM), lithology (14), structure (3) and land use (5). The percentage of the individual thematic variables in each mapping unit was computed in a GIS and used as independent variable in the statistical analysis. Very old landslides (A_0 in Table 7.1) were excluded from the analysis, and considered as additional explanatory variable describing rock strength.

A stepwise procedure was adopted to select the optimal landslide susceptibility model. Five separate statistical models were prepared using the same set of environmental variables and changing incrementally the landslide inventory map (Figure 7.4). The first model was prepared using solely the recent and the active landslides identified in the 1955 aerial photographs (A_1-A_2 in Table 7.1). The second model was obtained by adding the landslides identified in the 1975 aerial photographs (A_1-B_2). The same procedure was repeated adding the slope failures that were mapped in the 1980 (A_1-C_2), 1994 (A_1-D_2), and 1999 (A_1-E_2) aerial photographs. At each step, a different estimate of the probability of spatial landslide occurrence was obtained. The five susceptibility models were compared to establish statistical strength and geomorphological significance. Finally, the model prepared using the entire set of landslides inventoried in the period from 1954 to 1999 (A_1-E_2) was used to describe landslide susceptibility.

Table 7.2 lists the 36 thematic variables entered in the landslide susceptibility model. Variables strongly associated with the presence of landslides include slope (SLO_ANG2), mapping unit area (SLO_AREA), drainage channel order (ORDER), drainage channel mean slope (LNK_ANGKE), the presence of cultivated (SEM) and uncultivated areas (INC), and of pasture (PRA). Like in the Upper Tiber River basin (Table 6.3), landslide susceptibility increases with slope gradient to a threshold, above which it decreases (in Table 7.2 compare

the SDFC of SLO_ANG and SLO_ANG2). The overall percentage of mapping units correctly classified by the susceptibility model is 78.9% (Table 7.3).

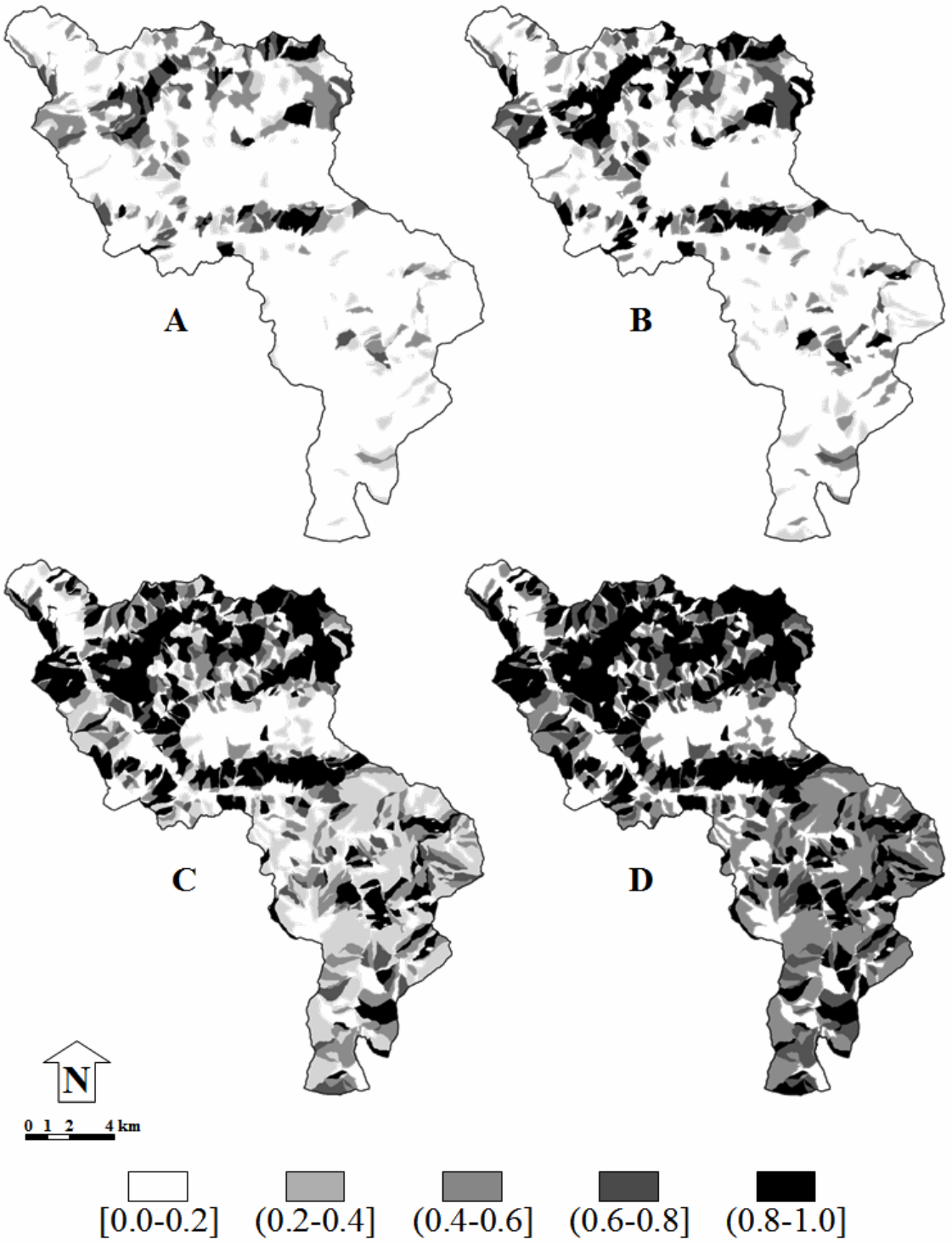

Figure 7.3 – Exceedance probability of landslide occurrence in the Staffora River basin obtained computing the mean recurrence interval of past landslide events from the multi-temporal inventory (Figure 7.1). Shades of grey show exceedance probability for different periods: (A) 5 years, (B) 10 years, (C) 25 years, (D) 50 years. Square bracket indicates class limit is included; round bracket indicates class limit is not included.

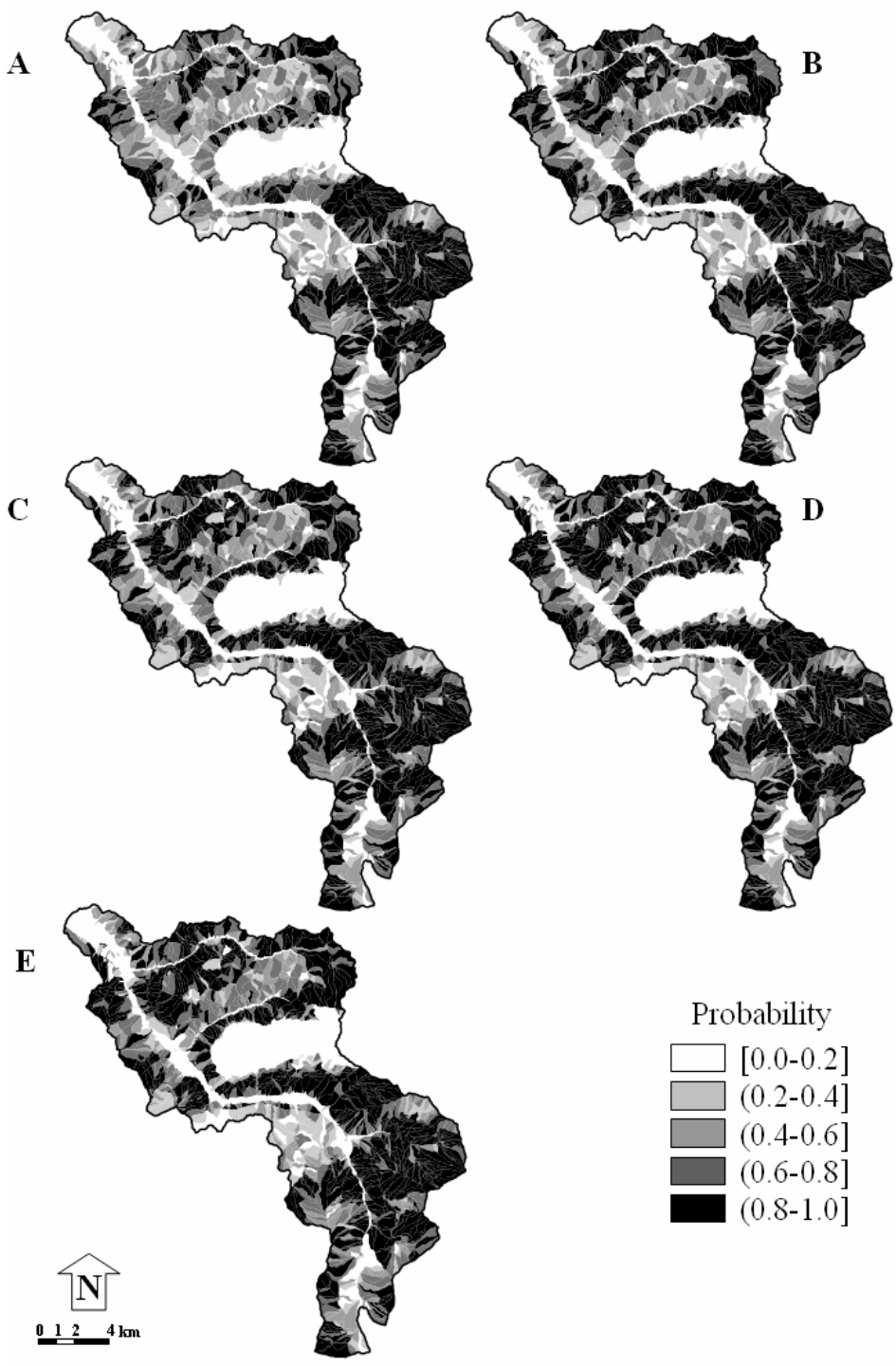

Figure 7.4 – Staffora River basin. Landslide susceptibility models obtained through discriminant analysis of the same set of independent thematic variables and changing the landslide inventory map (dependent variable, Figure 7.1 and Table 7.1). (A) using landslides identified in the period A_1–A_2; (B) using landslides in the period A_1–B_2; (C) using landslides in the period A_1–C_2; (D) using landslides in the period A_1–D_2; (E) using landslides in the period A_1–E_2. Shades of grey indicate spatial probability, in 5 classes. Square bracket indicates class limit is included; round bracket indicates class limit is not included.

Table 7.2 – Staffora River basin. Variables entered into the discriminant model as the best predictors of the occurrence of landslides in the 2243 geo-hydrological mapping units in which the basin was partitioned. Most important standardized discriminant function coefficients (SDFC) are shown in bold. Negative or positive sign of the coefficients indicates variables contributing toward stability (red) or instability (green), respectively.

	VARIABLES DESCRIPTION		*SDFC*
Morphology	Drainage channel magnitude	MAGN	.124
	Drainage channel order	ORDER	**-.232**
	Drainage channel length	LINK_LEN	-.119
	Mapping unit area	SLO_AREA	**-.246**
	Terrain unit micro-relief	R	.139
	Mapping unit mean elevation	ELV_M	.097
	Mapping unit mean slope angle	SLO_ANG	**-1.456**
	Mapping unit mean slope angle squared	SLO_ANG2	**1.265**
	Mapping unit mean slope angle standard deviation	ANG_STD	.190
	Drainage channel mean slope	LNK_ANG	**-.286**
	Mapping unit length standard deviation	LEN_STD	-.125
	Mapping unit slope (middle portion)	ANGLE2	.186
	Concave profile down slope	CONV	**.208**
	Concave-convex profile	COV_COC	.051
	Convex-concave profile	COC_COV	.150
	Rectilinear slope profile	RET	-.048
	Complex slope profile	CC	**.200**
Lithology	Recent alluvial deposit	ALLUVIO	**.592**
	Monte Vallassa sandstone	AR_BIS	**.441**
	Ranzano sandstone	AR_R_M_P	-.065
	Scabiazza sandstone	AR_SCA	-.063
	Detritus	DETRITO	-.099
	Monte Lumello marl	MR_AN_LO	.146
	Rigoroso marl	MR_B_R_C	.129
	Bosmenso marl	MR_BOSM	.051
	Monte Piano marl	MR_P_R_B	.122
Land use	Bare rock or soil	ALV	-.085
	Dense forest	BD	.048
	Woods	BMD	-.038
	Uncultivated area	INC	**-.281**
	Pasture	PRA	**-.222**
	Cultivated area	SEM	**-.277**
Structure	Bedding dipping into the slope	REG	.078
	Mapping unit facing N-NE	TR1	-.126
	Mapping unit facing S-SW	TR3	-.053
	Very old (relict) landslide (A_0)	FRA_OLD	-.053

As discussed in § 6.5, Table 7.3 provides a measure of the "degree of fitting" of the susceptibility model, i.e., of the ability of the model to predict the known distribution of (past) landslides. However, the contingency table does not prove the ability of the susceptibility model to predict the spatial occurrence of new (i.e., future) landslides. To obtain this, external (independent) information is required. The availability of the multi-temporal inventory map

allowed for a quantitative estimate of the prediction skill of the susceptibility model. To accomplish this, the total area of new landslides (at the date of the photographs) in each mapping unit was computed in the GIS. The obtained results were then compared with the susceptibility zoning obtained by the different discriminant models. Figure 7.5 relates the percentage of landslide area in each susceptibility class to the corresponding basin area, the latter ranked from most (left) to least (right) susceptible.

Table 7.3 – Staffora River basin. Comparison between mapping units classified as stable or unstable by the discriminant model (Figure 7.4) and mapping units free of and containing landslides in the inventory map (Figure 7.1).

		PREDICTED GROUPS (MODEL)	
		GROUP 0 *STABLE MAPPING UNITS*	*GROUP 1* *UNSTABLE MAPPING UNITS*
ACTUAL GROUPS (INVENTORY) *GROUP 0*	*MAPPING UNITS FREE OF LANDSLIDES IN INVENTORY MAP*	69.0 % (class 1)	31.0 % (class 3)
GROUP 1	*MAPPING UNITS CONTAINING LANDSLIDES IN INVENTORY MAP*	15.0 % (class 4)	85.0 % (class 2)

Overall percentage of mapping units correctly classified is 78.9%.

In Figure 7.5 four curves are shown, which portray different information. The blue dashed line and the green dotted line relate the percentage of landslide area used to prepare the model (past landslides, A_1-A_2 for model A, and A_1-B_2 for model B) to the predicted susceptibility. The continuous red line and the continuous violet line relate the cumulative percentage of landslide occurred after the model was prepared to the model prediction. While the first two curves (green and blue) measure model fit, the latter two curves (red and violet) provide a quantitative measure of the model ability to predict future landslides geographically. As expected, model fit (blue and violet lines) is better than model skill, which decreases with the increase of the time span of the prediction.

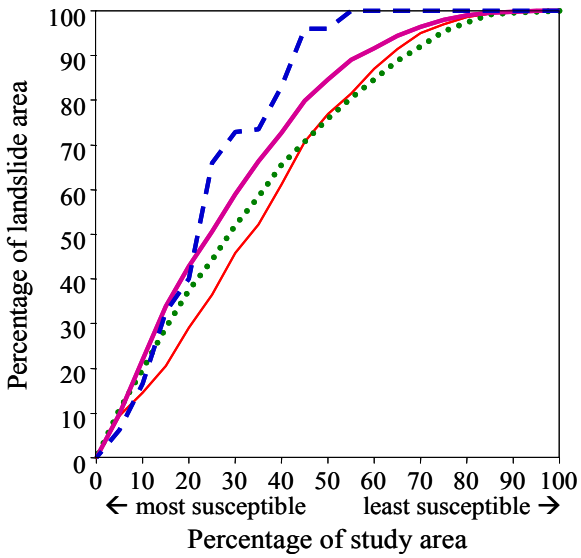

Figure 7.5 – Staffora River basin. Percentage of landslide area in each susceptibility class (y-axis) vs. the corresponding basin area (x-axis), ranked from most (left) to least (right) susceptible.

7.3.4. Hazard assessment

All the information needed to determine quantitatively landslide hazard in the Staffora River basin is now available, and the probability model introduced in § 7.2 can be applied. Figure 7.6 shows the workflow.

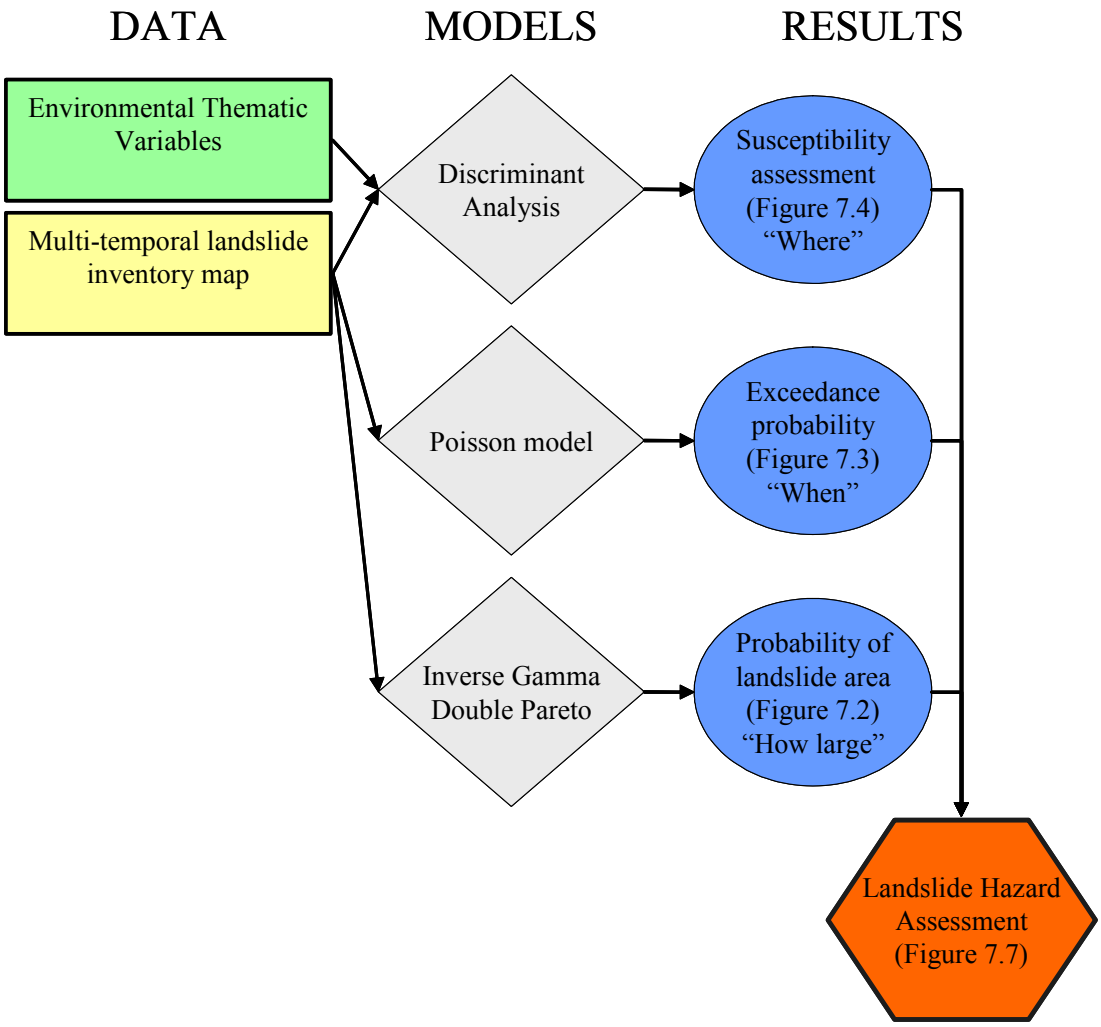

Figure 7.6 – Block diagram exemplifying the work flow adopted to determine landslide hazard. Rectangles indicate input data. Diamonds indicate individual models, for landslide susceptibility, for the temporal probability of landslides, and for landslide size. Ellipses indicate intermediate results. Hexagon indicates the final result.

Summarizing: (i) I obtained the probability of landslide size, a proxy for landslide magnitude, from the statistical analysis of the frequency-area distribution of the mapped landslides (eqs. 5.3 and 5.4, and Figure 7.2); (ii) I obtained the probability of landslide occurrence for established periods by computing the mean recurrence interval between successive failures in each mapping unit, and by adopting a Poisson probability model (equation 4.7, and Figure 7.3); and (iii) I obtained the spatial probability of slope failures (i.e., landslide susceptibility) through discriminant analysis of 46 environmental variables (equations 6.1 and 6.12, and Figure 7.4). Assuming independence, and multiplying the three probabilities, I obtain the landslide hazard, i.e., the joint probability that a mapping unit will be affected by future

landslides that exceed a given size, in a given time, and because of the local environmental setting (§ 7.2, equation 7.3).

Figure 7.7 shows examples of the obtained landslide hazard assessment. The Figure portrays landslide hazard for terrain units in the central part of the Staffora River basin for four periods (5, 10, 25 and 50 years), and for two landslide sizes, greater or equal than 2000 m^2 and greater or equal than one hectare.

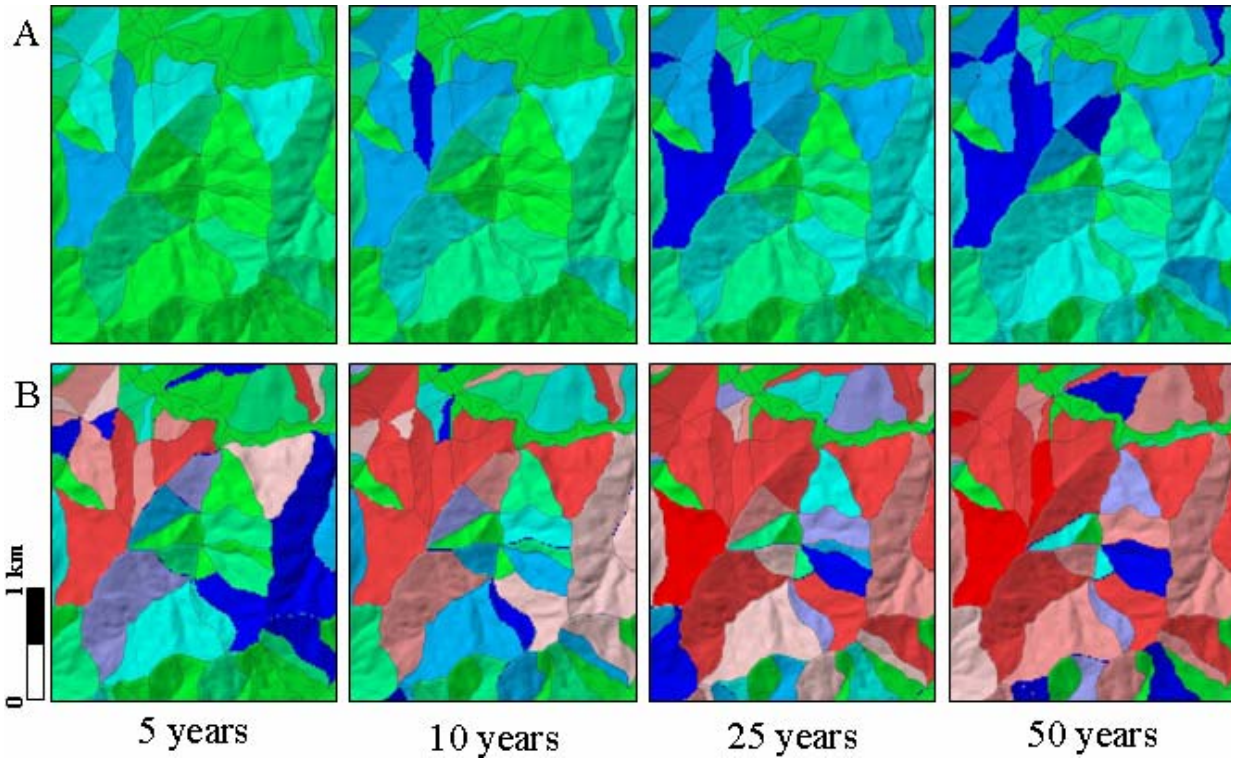

Figure 7.7 – Staffora River basin. Examples of landslide hazard maps for 4 periods, from 5 to 50 years, and for two landslide sizes, $A_L \geq 2000$ m^2 (A) and $A_L \geq 1$ ha (B). Colours show different joint probabilities of landslide size, of landslide temporal occurrence, and of landslide spatial occurrence.

7.3.5. Discussion

I now attempt a general discussion of the problems encountered and the results obtained in the assessment of landslide hazard in the Staffora River basin. Most importantly, I examine the validity of the assumptions under which the hazard assessment holds (§ 3.1, § 4.5, § 5.2, § 6.2.1). The discussion focuses on the experiment conducted in the Staffora River basin, but the framework and most of the conclusions are general, and applicable to other cases.

The obtained landslide hazard model holds under a set of assumptions, namely: (i) landslides will occur in the future under the same circumstances and because of the same factors that produced them in the past, (ii) landslide events are independent (uncorrelated) random events in time, (iii) the mean recurrence of slope failures will remain the same in the future as it was observed in the past, (iv) the statistics of landslide area are correct and will not change in the future, (v) landslide area is a reasonable proxy for landslide magnitude, and (vi) the probability of landslide size, the probability of landslide occurrence for established periods, and the spatial probability of slope failures, are independent.

That slope failures will occur in the future under the same conditions and because of the same factors that triggered them in the past is a recognized postulate for all functional (statistically based) susceptibility assessments (see § 6.2.1 and 6.4.1 for a discussion). As for the Upper Tiber River basin (§ 6.4), the main difficulty with this assumptions is that the environmental conditions (predisposing factors) that caused landslides "must remain the same in the future" in order to cause similar slope failures. It is reasonable to established (assume) a validity of the hazard model for the Staffora River basin of 50 years, approximately equivalent to the length of the period covered by the multi-temporal inventory used to establish landslide recurrence. Hence, the problem is that of investigating the possibility that the predisposing factors will change in the next 50 years, changing landslide susceptibility.

It is safe to assume that geological factors (e.g., lithology, structure, seismicity) will not change (significantly) in such a short geological time. Local morphological modifications can occur in the period due to stream erosion, landslides and human actions, but extensive morphological changes are not reasonably foreseeable. If significant changes should occur, the susceptibility model should be rejected or revaluated. Inspection of Table 7.2 reveals that 30 of the 36 thematic variables entered into the susceptibility model are not expected to change significantly in the considered period. However, variables describing land use types may change, locally significantly, and changes in land use are known to affect landslide frequency and abundance (Guthrie, 2002; Glade, 2003). Quantitative estimates of land use change are not available for the Staffora River basin, although they could be obtained by interpreting and comparing the available sets of aerial photographs. Qualitative estimates indicate a reduction of about 25% of the forest coverage in the period from 1955 to 1999, in favour of cultivated land. In the same period, agricultural practices have changed, largely aided by powerful mechanical equipments. If land use will change considerably in the Staffora River basin, the role of some the environmental variables considered in the susceptibility model will also change, hampering the validity of the model. A new model should be prepared, considering variables showing areas of land use change.

The adopted susceptibility model does not consider the landslide triggering factors, i.e., rainfall, seismic shaking or snow melting. Changes in the frequency or intensity of the driving forces will not affect (at least not in the considered period) the susceptibility model. However, the changes may affect the rate of occurrence of landslide events.

In the Apennines, evidence exists that where abundant clay, marl and sandstone crop out landslides exhibit spatial persistence, i.e., landslides occur more abundantly where they occurred in the past (Cardinali *et al.*, 2000, § 4.4). If this is the case for the Staffora River basin, the assumption that landslide events are uncorrelated random events in time may be violated. Analysis in a GIS of the multi-temporal inventory reveals that 40% of all the landslides identified in the period from 1955 to 1999 (A_2–E_2 in Table 7.2) occurred inside landslide areas mapped on the 1955 aerial photographs (A_0–A_1). Considering only the 2390 landslides occurred in the 45-year period from 1955 to 1999 (A_2–E_2), 12% of the slope failures occurred in the same area of other landslides occurred in the same period. For the Staffora River basin, an archive inventory of historical landslide events covering the period from 1850 to 1998 is available. Analysis of the information listed in this inventory indicates that 389 landslide events occurred at 332 different sites, with only 38 sites affected two or more times. The same landslide site was affected on average 1.2 times, indicating a low rate of recurrence of events at the same site. All this concurs to establish that for the period of the hazard assessment (i.e., 50 years) in the Staffora River basin landslides can be considered uncorrelated random events in time.

Analysis of the archive inventory provides information also on the triggering mechanisms of the slope failures. Of the 248 landslide events listed in the catalogue for which the triggering mechanism is known, 210 (84.7%) were the result of intense rainfall, 16 (6.5%) to a combination of intense rainfall and snow melting, infiltration, irrigation or broken pipes, 14 (5.6%) to erosion at the base of the slope, and eight (3.2%) to other causes. The analysis indicates that most of the landslides in the Staffora River basin are rainfall induced. If the rate of occurrence of the meteorological events that trigger landslides changes, the mean rate of slope failures will also change. If the intensity (amplitude and duration) of the rainfall will change, the rate of slope failures might change, in a way that is not predictable. For the coming decades, south of the Alps models of global climate change forecast the same total amount of yearly rainfall concentrated in a fewer number of high intensity events (Bradley *et al.*, 1987; Brunetti *et al.*, 2000; Easterling *et al.*, 2000; IPCC, 2001). This may result in more abundant shallow landslides and in less frequent deep-seated slope failures (Buma and Dehn, 1998; Dehn and Buma, 1999). Modifications in land use induced by changes in agricultural practices may also locally change the rate of occurrence of landslides.

As I have shown in § 5, determining the statistics of landslide area is no trivial task (Guzzetti *et al.*, 2002b; Malamud *et al.*, 2004a). The (scant) available literature (Stark and Hovius, 2001; Guzzetti *et al.*, 2002b; Guthrie and Evans, 2004a,b; Malamud *et al.*, 2004a,b) seems to indicate that the frequency-area statistics of landslide areas does not change significantly across lithological or physiographical boundaries. Malamud *et al.* (2004a) showed that three different populations of landslides produced by different triggers (i.e., seismic shaking, intense rainfall, rapid snow melting) in different physiographical regions (southern California, central America, central Italy), exhibit virtually identical probability density functions. Data available for Umbria indicates that the probability density of landslide area does not change significantly with time. It is therefore safe to assume that in the Staffora River basin the frequency-area statistics of landslide area will not change in the period considered for the hazard assessment. It is also justified to use a single probability density function for the entire basin.

Hungr (1997) argued that no unique measure of landslide magnitude is available, and proposed to adopt destructiveness as a measure of landslide magnitude. In the Staffora River basin, landslide area was taken as a proxy for landslide destructiveness and of landslide magnitude. The area of the individual landslides was obtained in a GIS from the multi-temporal inventory. However, it is not established in the Staffora River basin that landslide area is necessarily a good measure of landslide destructiveness. Analysis of the archive inventory reveals that information on the size (area, length and width) of landslides is available for 26 events (6.7%), which range from 600 m^2 to 0.6 km^2 (mean = 5.8 ha, std. dev. = 13.5 ha). Damage caused by these landslides was mostly to the roads and subordinately to private homes and to the aqueduct. Information on landslide type is available for 28 events (7.2%), of which 15 were slides, 6 flows and 5 falls. Slides and flows caused the most severe damage, and falls produced only minor, temporary interruptions along the roads. Information on landslide velocity is available for five events, and ranges from 10 cm/h to 1 m/day. The ensemble of the historical information on damaging slope failures indicates that damage in the Staffora River basin is caused mostly by slow to rapid moving slides and flows (i.e., the type of failures considered in the hazard assessment), and that large landslides tend to produce larger damage.

The last assumption of the proposed model is that the probabilities of landslide size, of temporal occurrence, and of spatial incidence of mass movements are all independent. The

legitimacy of this assumption is difficult to prove. As previously shown, in the Staffora River basin the probability of landslide area is largely independent from the physiographical setting. Hence, the probability of landslide area is independent from landslide susceptibility. The susceptibility model was constructed without considering the driving forces (meteorological or others) that control the rate of occurrence of slope failures in the basin. Thus, the rate of landslide events is largely independent from landslide susceptibility. Lastly, analysis of the information listed in the archive inventory revealed that slope failures occurred in all sizes, indicating that the rate of failures is independent from landslide size. Finally, the hazard model has produced many hazard maps, one for any of the many possible landslide scenarios (e.g., different landslide sizes, different return periods, etc.). How to combine this large number of maps into a single product useful to decision makers remains an open problem (§ 9.4).

7.4. Assessment of landslide hazard at the national scale

Establishing the level of landslide hazard for an entire nation is a difficult task, and only a few – largely empirical – attempts have been pursued (e.g., Radbruch-Hall *et al*., 1982; Brabb *et al*., 1999). The main difficulty of such attempts lies in the scant availability of relevant information for territories extending for hundreds of thousands of square kilometres. In Italy, relevant information is available to attempt a quantitative assessment of landslide hazard using a modified version of the probability model presented in § 7.2. The model requires three probability estimates, namely: (i) of the spatial probability of landslides (i.e., susceptibility), (ii) of the temporal occurrence of landslides, and (iii) of the magnitude (or the destructiveness) of the expected landslide event. Preliminary to the definition of landslide hazard is the selection of an appropriate mapping unit. For this experiment, the municipality (an administrative and political subdivision, § 6.2.2) is selected as the terrain partitioning unit. Italy is divided into 8102 municipalities, ranging in size from 1285 km^2 (Rome) to 0.11 km^2 (Atrani, Campania) (mean area = 37.3 km^2, mode = 26.25 km^2, std. dev. = 50.00 km^2).

7.4.1. Spatial probability of landslide events

Landslide susceptibility in each municipality was ascertained through discriminant analysis of independent thematic variables describing morphometry, hydrology, lithology and soil types (§ 2.1). Morphometric and hydrological variables were obtained in a raster GIS from the 90 m × 90 m DEM acquired by the Shuttle Radar Topography Mission (SRTM) in February of 2000. Lithological information was obtained from a synoptic geological map published by Compagnoni and his collaborators, in the period from 1976 to 1983. For the statistical analysis, the large number of rock units shown in the synoptic geological map (145 units) was grouped into 20 lithological types. Similarly, the 34 soil types shown in the synoptic soil map of Mancini (1966) were grouped into 8 classes of soil thickness and 11 classes of soil parent material. As a dependent variable, the presence/absence of historical landslide events listed in the archive inventory of the AVI project (see § 3.3.1.1) was used. Figure 7.8 shows the result of the susceptibility assessment.

7.4.2. Probability of event occurrence

To establish the recurrence of the landslide events, and to estimate the probability of landslide occurrence in an established period, the archive inventory compiled by the AVI project was used (§ 3.3.1.1). This inventory lists 22,547 landslide events in the period between 1900 and 2001. In each municipality, the average recurrence of landslide events was obtained dividing

the total number of events listed in the historical catalogue (from 0 to 353) by the time span of the investigated period (102 years, from 1900 to 2001). Assuming that the recurrence of landslides will remain the same for the future and adopting a Poisson probability model (§ 4.5), the exceedance probability of having one or more damaging landslide event in each municipality was established for different periods, from 5 to 100 years.

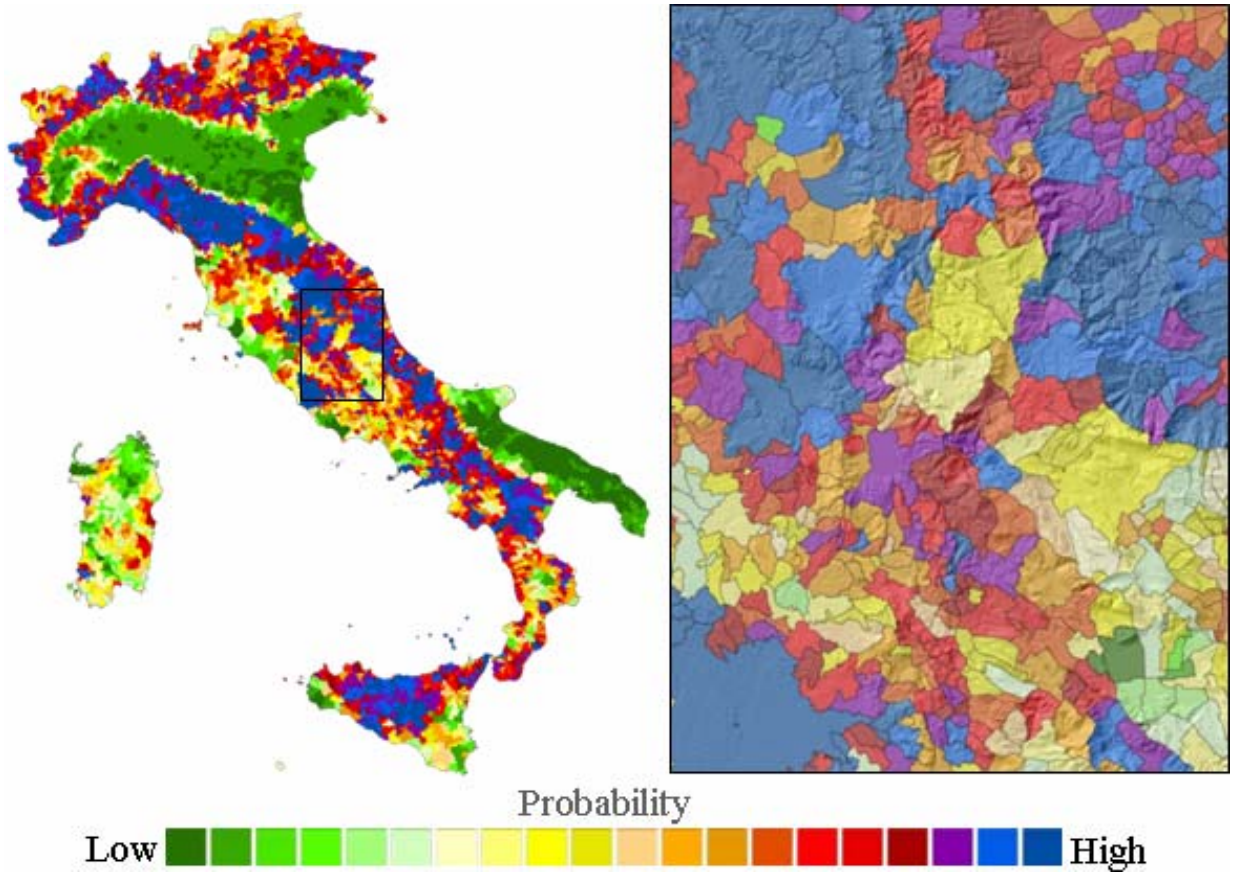

Figure 7.8 – Landslide susceptibility map of Italy, obtained through discriminant analysis of morphometric, hydrological, lithological and soil information. Mapping unit is the municipality. Probability of landslide spatial occurrence shown in 20 classes, from low (dark green) to high (dark blue).

7.4.3. Probability of the consequences

The probability model of landslide hazard requires an estimate of the magnitude of the expected events. No direct information on the statistics of the magnitude of landslides is available for Italy. In the archive inventory, the size (length, area, volume) or the velocity of the slope failures is known for a small number of events, preventing the use of these parameters as proxies of landslide magnitude. Salvati *et al.* (2003) compiled a catalogue of historical landslide (ad flood) events that resulted in deaths, missing persons, injuries and homelessness in the period from AD 1279 to 2002. Guzzetti *et al*. (2005b,c) used this catalogue to study the consequences of the damaging landslide events, including a quantitative estimate of societal risk (§ 8.3.1.2). Societal risk was obtained through the analysis of the frequency statistics of historical landslides with human consequences. The latter is a

quantitative measure of the destructiveness to the population caused by landslide events, and can be conveniently used as a proxy for landslide magnitude.

7.4.4. Hazard assessment and discussion

The information needed to establish landslide hazard is now available. To define the hazard the proposition given in equation 7.2 has to be slightly modified. Here, I define landslide hazard (at the national scale) as:

$$H_L=P[P(C) \geq 1 \text{ in a time interval } t, \text{ given } \{\text{morphology, lithology, soil types,...}\}] \quad (7.4)$$

where, P_C is the probability of the consequences of a landslide event, measured by the number of fatalities caused by the event. For any given municipality, equation 7.4 expresses landslide hazard has the conditional probability of landslide damage to the population, $P(C)$, of landslide occurrence in an established period t, $P(N_L)$, and of landslide spatial occurrence (S), given the local environmental setting. Assuming independence, the landslide hazard, i.e., the joint probability, is:

$$H_L = P(C) \times P(N_L) \times S \quad (7.5)$$

where, the probability of landslide damage to the population was obtained from the catalogue of landslides with human consequences, the probability of landslide events occurrence was established from the archive inventory of landslide events in Italy, and the probability of landslide events spatial occurrence was obtained though discriminant analysis of morphometric, hydrological, lithological and soil information. Figure 7.9 shows schematically how landslide hazard was obtained.

To establish susceptibility, the presence / absence of historical events in each municipality was selected as the dependent variable. Clearly, local incompleteness in the archive inventory or errors in positioning historical landslide events affect the susceptibility model. Also, the abundance of historical events in each municipality was not considered in the susceptibility model. The independent variables were selected mostly from two thematic layers (the synoptic geological and soil maps) and a DEM. The relationship between this information and the location of historical landslide events in the municipalities was not established independently. Additional independent variables were obtained from the archive landslide inventory, including the density of the events (i.e., number of events in the municipality / area of the municipality). However, the percentage of the municipality that could be affected by landslides was not considered when computing the density. Land use and its changes, which are known to affect landslides, were not considered in the model, as were not considered changes in the population and its density distribution.

To establish the recurrence of landslide events in each municipality, the archive inventory of landslide events in Italy was used (§ 3.3.1.1). Incompleteness in this catalogue will affect the probability of landslide events and the hazard model. To establish the probability of the consequences, the catalogue of landslides which resulted in deaths, missing persons, injured and homeless people, was used. Incompleteness of this catalogue will affect the probability of the consequences and the final hazard model. Also, independence between the historical landslide events and the events with consequences to the population has not been established.

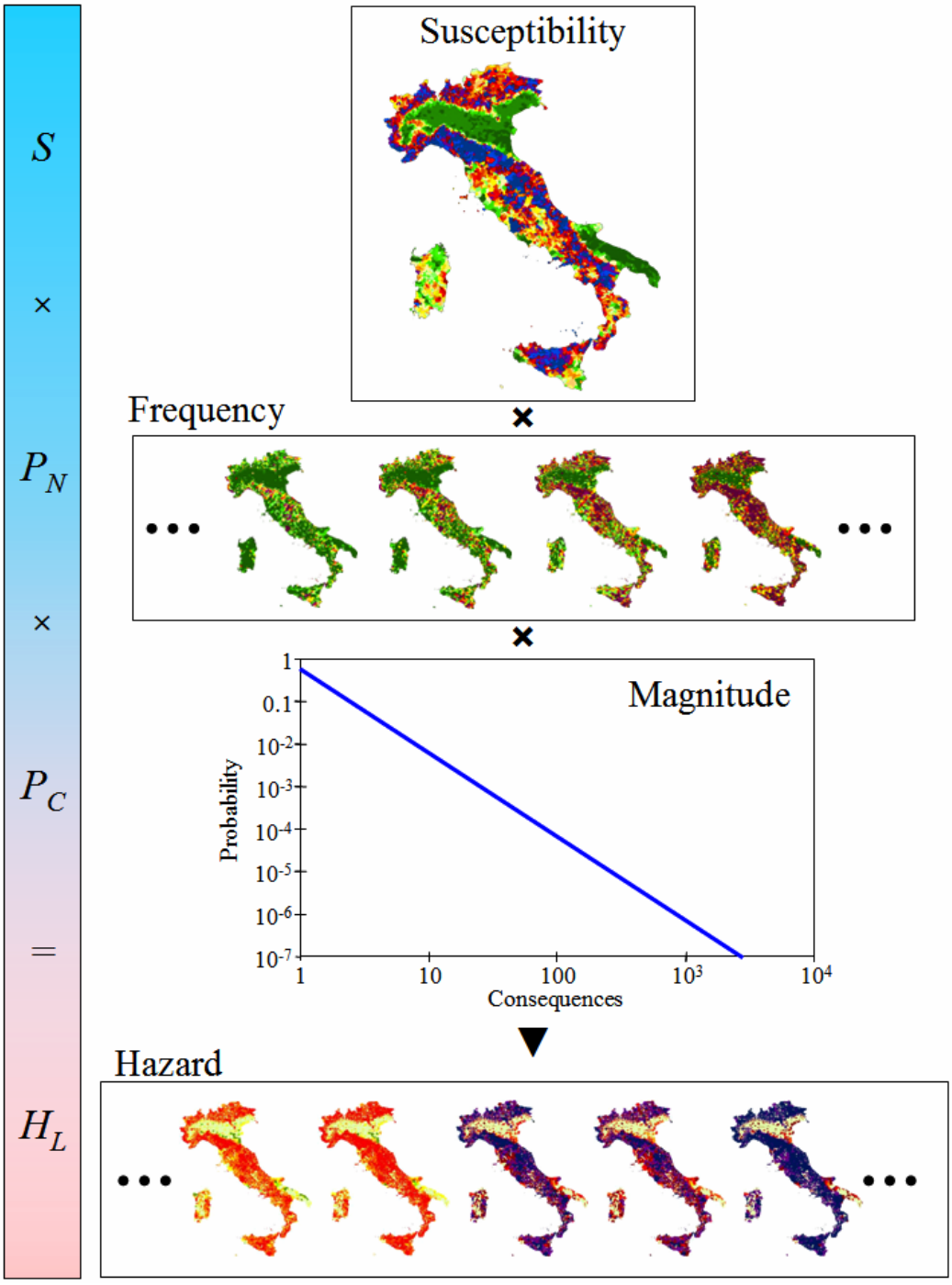

Figure 7.9 – Schematic representation of the procedure adopted to evaluate landslide hazard at the national scale, in Italy.

As in the case of the Staffora River basin (§ 7.3), the hazard model has produced (or can produce) many different hazard maps, one for any of the several possible landslide scenarios (e.g., different expected number of fatalities, different return periods, etc.). How to combine the large number of maps into a product useful to decision makers remains an open problem (§ 9.4).

The obtained assessment is the first quantitative and reproducible estimate of landslide hazard available for Italy, at the national (synoptic) scale. The model is functional (i.e., statistical), and its quality depends (almost) entirely on the quality, completeness and relevance of the input data. Most vitally, the validity and limitations of the basic assumptions on which the probabilistic model was developed were not proven for this national hazard assessment. This is not an easy task that requires further investigation.

7.5. Rock fall hazard assessment along the Nera and Corno valleys

Rock fall is a common-place geomorphological process and represents a major hazard in mountain areas worldwide (Whalley, 1984; Flageollet and Weber, 1996). Rock falls range in size from small cobbles to large boulders of hundreds of cubic meters, travel at speeds ranging from few to tens of meters per second, and for long distances from the detachment zone to the deposition area (Cruden and Varnes, 1996). Despite their often relatively small size, rock falls are among the most destructive mass movements (Whalley, 1984; Rochet, 1987, Evans and Hungr, 1993; Evans, 1997), and in Italy they represent a primary cause of landslide fatalities (Guzzetti, 2000; Guzzetti *et al.*, 2005c).

The size and speed of rock falls, and their ability to travel long distances (exceeding one kilometre) makes the previously discussed methods to ascertain landslide hazard largely unsuitable to rock falls. In particular, it is the subdivision of terrain based on slope units or geo-hydrological units that is largely incompatible with this landslide type. A boulder detached from a rock cliff can travel across geo-hydrological or slope unit boundaries. Rock fall susceptibility and hazard are not related only to where rock falls occur (i.e., where they detach), but also to where rock falls travel and deposit. For rock falls, quantitative measures of their magnitude are possible. Knowing the mass of the falling boulder (i.e., the volume × the rock density) and its velocity, kinetic or potential energy can be easily computed, which represent a direct measure of the magnitude of the event, a good proxy for destructiveness. If the size of the boulder is undetermined, velocity can be selected as a reasonable proxy for magnitude.

In the following, I describe a quantitative attempt to determine rock fall hazard along the Nera River and the Corno River valleys, in south eastern Umbria (§ 2.5). The attempt is based on the use of the computer programme STONE (Guzzetti *et al.*, 2002), which I briefly describe below..

7.5.1. The computer program STONE

To assess rock fall hazard, knowledge on the spatial (geographical) distribution of the expected rock falls is essential. To obtain this information, I contributed to develop STONE (Guzzetti *et al.*, 2002), a computer program capable of simulating rock fall processes in three-dimensions. STONE uses a lumped-mass approach to simulate rock fall processes. The falling boulder is considered dimensionless and a kinematic simulation is performed. The input data required by STONE include: (i) the location of the detachment areas of rock falls, (ii) the number of boulders launched from each detachment area, (iii) the starting velocity and horizontal angle of the rock fall, (iv) a velocity threshold below which a boulder stops, (v) a DEM describing topography, and (vi) the coefficients of dynamic rolling friction, and of normal and tangential energy restitution used to simulate the loss of energy where the boulder

is rolling and at the impact points. The latter variables are provided as raster maps, i.e., in a spatially distributed format.

STONE is capable of coping with the uncertainty and the inherent variability in the required input data. The software accomplishes this in two ways: (i) by launching a variable number of blocks from each detachment cell, and (ii) by varying randomly the starting horizontal angle, the dynamic rolling friction coefficient, and the normal and tangential energy restitution coefficients. The software uses GIS technology to produce 2- and 3-dimensional rock fall trajectory lines and raster maps. The latter include three grids portraying: (i) the cumulative count of rock fall trajectories that pass through each cell, (ii) the maximum computed velocity, and (iii) the largest distance of the boulder to the ground computed along the rock fall trajectories (flying height) (Guzzetti *et al.*, 2002). The three grid maps can be used to attempt to ascertain rock fall hazard.

7.5.2. Application of the rock fall simulation model

I used the computer program STONE in a 48 km^2 area along the Nera River and the Corno River valleys centred on the town of Triponzo (§ 2.5). In this area rock falls are frequent and dangerous. In the 1980's, a new tunnel was constructed along State Road 320 to bypass the Balza Tagliata gorge, east of Triponzo, where rock falls were particularly frequent and hazardous, and a section of the road was abandoned. In October 1997, earthquake shaking triggered several rock falls in the study area. The earthquake induced landslides were particularly abundant along the Balza Tagliata gorge (§ 3.3.3.3).

Data used by STONE to complete the spatially-distributed rock fall simulation were described in § 2.5, and were obtained from: (i) existing topographic and geological maps, (ii) the interpretation of two sets of aerial photographs flown in July 1977 and in October-November 1997, and (iii) field surveys. A DEM with a ground resolution of 5 m × 5 m was obtained by interpolating 10 and 5 meter interval contour lines obtained from the 1:10,000 scale base maps. The source areas of rock falls were mapped on the same topographic maps at 1:10,000 scale from vertical aerial photographs at 1:13,000 and 1:20,000 scale, and then checked in the field. Oblique aerial photographs taken with a handheld camera from a helicopter immediately after the September-October 1997 earthquakes (§ 3.3.3.3) were used to refine the mapping locally. Minor rock slopes and road cuts from which rock falls can occur were mapped in the field. A total of 2.0 km^2 of rock fall source areas were identified. This corresponds to about 4.2% of the study area. Correcting for the steep topographic gradient, rock fall detachment areas extend for approximately 3.0 km^2.

Variables controlling the loss of energy at impact points (normal and tangential energy restitution coefficients) and where a boulder is rolling (dynamic friction angle) were obtained by recoding a surface geology and landslide inventory map prepared by updating the existing large-scale geological and landslide maps, mostly through the analysis of aerial photographs (Antonini *et al.*, 2002a, b). For each lithological unit cropping out in the study area, values of the dynamic friction angle and of the normal and tangential energy restitution coefficients were obtained from the literature (Broili, 1973; ERM-Hong Kong, 1998; Fornaro *et al*., 1990, Azzoni *et al.*, 1995; Crosta and Agliardi, 2000; Chau *et al.*, 2003) and from the personal experience in the use of the computer program STONE. Table 7.4 summarizes the values of the dynamic rolling friction angle, and the normal and tangential energy restitution coefficients assigned to each terrain type.

Definition of the values shown in Table 7.4 was inevitably heuristic, and to some extent arbitrary. Where bedrock crops out, and in the source area of rock falls, boulders do not loose much energy at impact point and where rolling. To these areas are assigned high values of the normal (55-65) and tangential (65-75) energy restitution coefficients, and low values of the dynamic rolling friction angle (0.25-0.40). The ranges of values reflect variations in the rock types. Massive and thickly layered limestone is assigned very high values of the energy restitution coefficients and very small values of the dynamic rolling angle. Thinly bedded limestone, marl and clay are assigned intermediate values of the normal and tangential restitution coefficients and larger values of the dynamic rolling angle. Field surveys revealed that only few boulders reached the areas where alluvial deposits crop out along the valley bottoms. Where this occurred, the boulders did not travel far. Based on this finding, alluvial deposits are assigned very low values of the normal (15) and tangential (30) energy restitution coefficients, and a very high value of the dynamic rolling friction angle (0.80). To the other terrain types are assigned intermediate values of the normal and tangential energy restitution coefficients and of the dynamic rolling friction angle, based on the hardness and the roughness of the topographic surface.

Table 7.4 – Nera River and the Corno River valleys. Values of the dynamic-rolling friction angle and of the normal and tangential energy restitution coefficients assigned to each terrain type. A range of ± 5% of the value was adopted to account for uncertainty in the coefficients.

Terrain type	*Rolling friction Value*	*Normal restitution Value*	*Tangential restitution Value*
Alluvial deposit	0.80	15	30
Alluvial fan	0.60	25	55
Debris cone	0.60	30	50
Debris deposit	0.70	35	55
Shallow debris deposit	0.70	35	60
Talus	0.65	35	55
Landslide deposit	0.40	45	55
Landslide crown area	0.35	55	65
Debris flow deposit	0.65	30	55
Debris flow source area	0.55	35	60
Massive and thickly layered limestone, and Travertine	0.30	65	75
Rock fall source area in massive and thickly layered limestone, and Travertine deposit	0.25	65	75
Thinly bedded limestone, cherty limestone	0.35	60	70
Rock fall source area in thinly bedded, cherty limestone	0.30	60	70
Marly limestone, marl and clay	0.40	55	65
Rock fall source area in marly limestone, marl and clay	0.35	55	65

The spatially distributed rock fall model for the Nera River and the Corno River valleys is the result of an iterative procedure. A preliminary model was produced by launching a single ("virtual") boulder from each rock fall source cell. The map of the rock fall count was visually inspected and checked with the location of known rock falls and the extent of talus, landslide and other debris deposits. Model variables were adjusted to avoid unreasonable results. The process was repeated a number of times, changing the model parameters and the initial conditions (i.e., the starting velocity, the impact and friction coefficients, etc.) until the result was judged satisfactory. A second model was then produced by launching 30 boulders from each source cell, and by allowing the model variables to vary randomly within five percent of the pre-defined average values (Table 7.4). This allowed considering the effects of the

variability of the rock fall process and the unpredictability in the modelling variables. Finally, the number of rock falls launched from each detachment cell was varied according to the rock type of the source area. In particular, where massive or thickly layered limestone and travertine deposits crop out, 50 blocks were launched, where thinly bedded limestone and cherty limestone crop out 45 boulders were launched, and where thinly bedded marly limestone, marl and clay crop out 35 boulders were launched.

Figure 7.10.A shows the resulting map of the cumulative count of the expected rock fall trajectories, and Figure 7.11 shows a 3-dimensional view of a portion of the same map. In the two figures, the spread of colours indicates a variable number of expected rock falls, from very few (1-10, green) to numerous (> 500, dark violet).

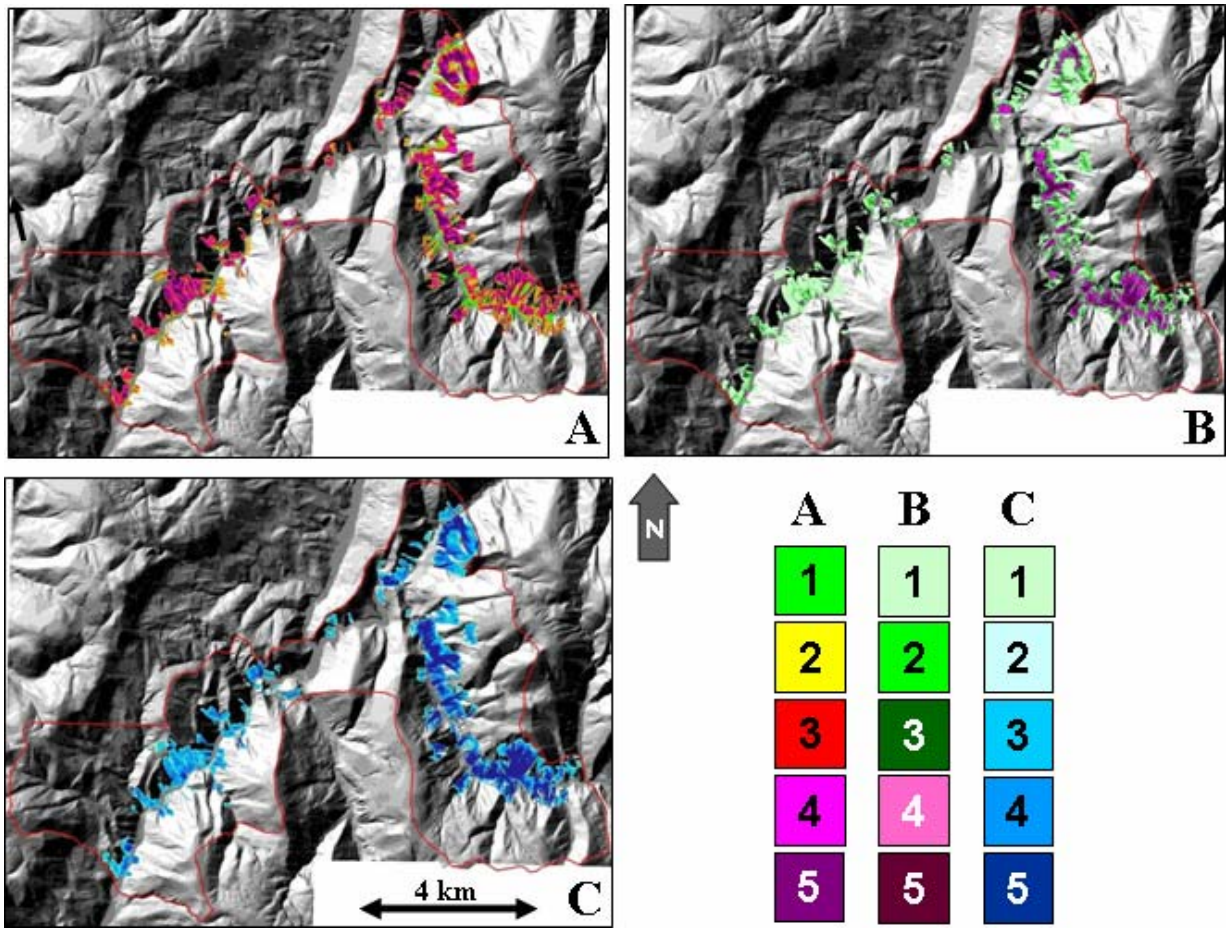

Figure 7.10 – Rock fall maps produced by STONE for the Nera River and the Corno River valleys. (A) cumulative count of rock fall trajectories; 1) 1-10 blocks, 2) 11-100 blocks, 3) 101-250 blocks, 4) 251-500 blocks, 5) > 500 blocks. (B) map of the maximum rock fall flying height; 1) < 1m, 2) 1-5 m, 3) 5-10 m, 4) 10-30 m, 5) > 30 m. (C) map of the maximum rock fall velocity; 1) < 1.5-25 km/h, 2) 25-40 km/h, 3) 40-70 km/h, 4) 70-115 km/h, 5) > 115 km/h.

As expected, the frequency of rock falls is not the same throughout the study area. Rock falls are most abundant along steep channels and drainage lines, confirming the field observation that topography locally controls rock fall trajectories. The map of the count of the expected rock falls can be compared with the extent of the talus, landslides, and other debris deposits, and with the location of rock falls triggered by the 1997 earthquake sequence (§ 3.3.3.3).

Comparison with the extent of talus deposits reveals that only at few places the map of the rock fall count exceeds down-slope the extent of the talus deposits. In places this occurs where the lower limit of the talus corresponds to the flat part of the valley bottom. Comparison with the location of the earthquake-induced failures reveals that the extent of the expected rock fall areas and the frequency of rock fall trajectories are in good agreement with the available information on known rock fall events. Of the 109 known rock fall deposits, 98 (89.9%) are located in areas where rock falls are expected, and 11 (10.1%) occur in areas where rock falls are not expected. This is an efficient form of model validation. A final model validation was performed by randomly inspecting the distribution of the vertical distance of the rock fall trajectories (Figure 7.10.B) (flying height, i.e., the distance of the boulder to the ground) and of the rock fall maximum velocity (Figure 7.10.C). Results indicate that the computed rock fall velocity locally exceeds 250 $km \cdot h^{-1}$ and the computed rock fall flying height ranges from zero, where boulders are rolling, to more that 165 metres above the ground, near high cliffs.

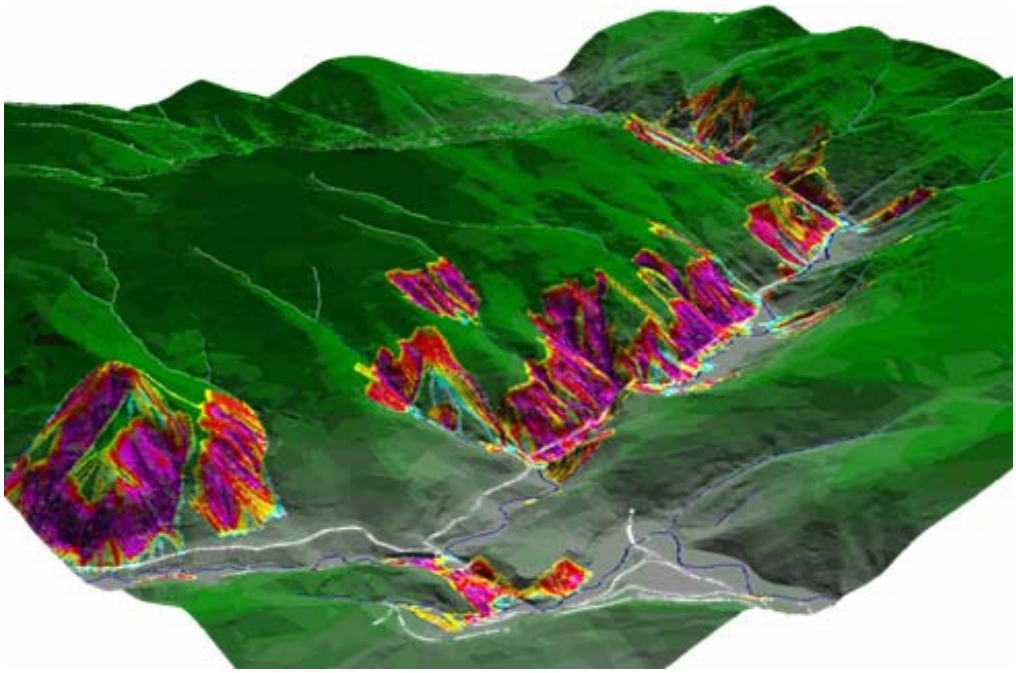

Figure 7.11 – Triponzo area, along the Nera River and the Corno River valleys. Three-dimensional view of a portion of the grid map showing the count of rock fall trajectories (Figure 7.10.A). Colours indicate increasing number of rock fall trajectories, from few (light blue) to very many (dark violet).

7.5.3. Rock fall hazard assessment

The three raster maps produced by STONE and discussed before can be used to ascertain rock fall hazard along the Nera River and the Corno River valleys. The map showing the total number of rock fall trajectories (Figure 7.10.A) can be considered a convenient proxy for the expected frequency of rock fall occurrence. For each grid cell the count of rock fall trajectories is a proxy for the probability of being struck by a falling or rolling boulder. The larger the number of computed trajectories, the higher the expected frequency of rock fall occurrence. Maps of the largest distance to the ground (Figure 7.10.B) and of the highest computed velocity (Figure 7.10.C) provide information on the intensity of the expected rock fall, a proxy for the maximum kinetic energy at each grid cell (Guzzetti *et al.*, 2002).

To determine rock fall hazard, I adopt a heuristic approach. I assume that rock fall hazard, H_{RF}, is a linear combination of rock fall count (c), maximum rock fall flying height (h), and maximum rock fall velocity (v), or

$$H_{RF} = f\,(c_{RF},\, h_{RF},\, v_{RF}) \tag{7.6}$$

Levels of rock fall hazard are attributed using a three-digit positional index, similar to that proposed by Cardinali *et al*. (2002) (§ 8.4.6, § 8.4.8). In the index, the left digit refers to the rock fall count (c_{RF}), the central digit to the rock fall flying height (h_{RF}), and the right digit to the rock fall velocity (v_{RF}). The index expresses rock fall hazard by keeping the three components of the hazard distinct from one another. This facilitates hazard zoning by allowing to understand whether the hazard results from a large number of expected rock falls (i.e., high frequency), a large intensity (i.e., high flying height or high velocity), or some combination of the three.

Figure 7.12 shows the final rock fall hazard map for the Nera River and the Corno River valleys. For display purposes, the original 125 rock fall hazard classes (5 classes of rock fall counts × 5 classes of rock fall flying height × 5 classes of rock fall velocity) were reduced into a more manageable number of classes (5), adopting a simple scheme.

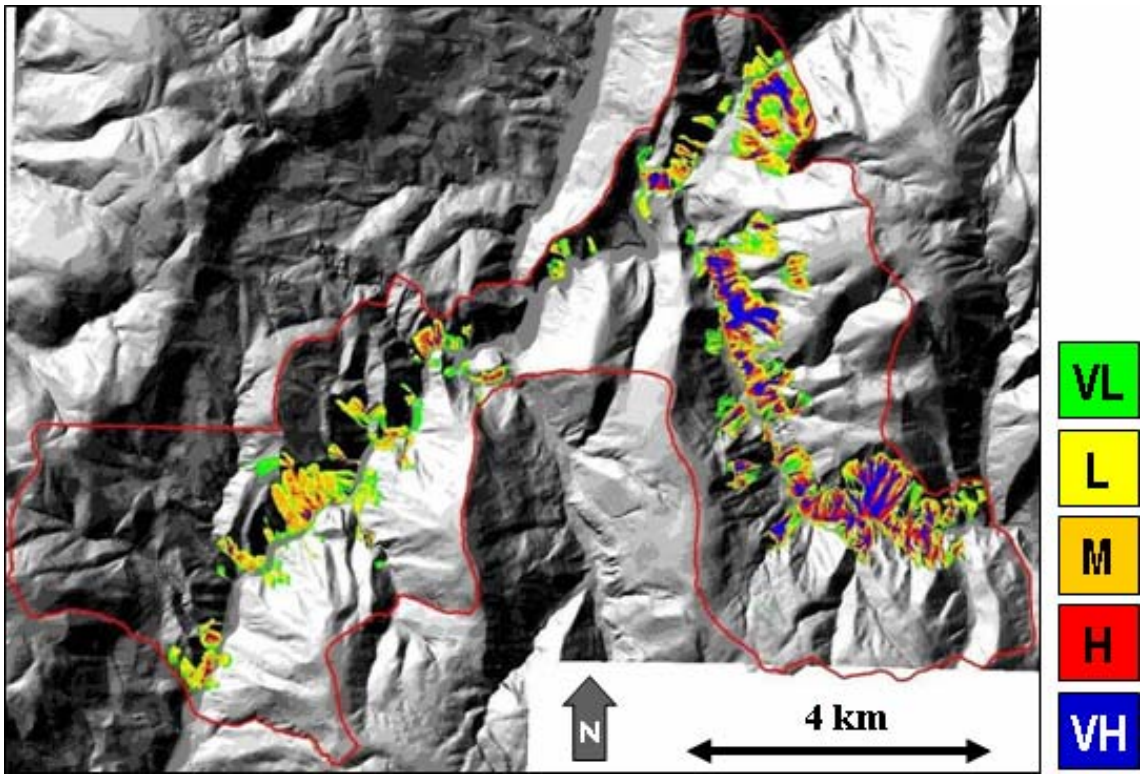

Figure 7.12 – Rock fall hazard map for the Nera River and the Corno River valleys. Legend: VL, very low hazard, L, low hazard, M, intermediate hazard, H, high hazard, VH, very high hazard.

Analysis of the hazard map reveals that 7.0 km^2 (in plan view) of the study area may be affected by rock falls. This corresponds to 14.6% of the area, including 2.0 km^2 of rock fall detachment zones. Correcting for the steep topographic gradient (obtained from the DEM), the area affected by rock falls extends for about 9.5 km^2. Inspection of Figure 7.12 reveals that

rock fall hazard is not distributed uniformly. About 3.4 km^2 of the study area (in plan view) are subject to low (25.5%) or very low (23.0%) hazard, 1.5 km^2 (22.2%) are subject to intermediate hazard conditions, and 2.0 km^2 are subject to high (15.3%) or very high (14.0%) hazard.

By overlaying the rock fall hazard map with the map of the transportation network in a GIS, the sections of the roads potentially subject to rock falls can be identified. Of the 31.8 km of paved roads in the study area, 9.0 km (28.5%) are found to be potentially affected by rock fall hazard.

Comparison of the hazard map with the location of the earthquake-induced rock fall events in 1997 reveals that 72.5% of the seismically induced rock falls occurred in areas where the hazard is expected to be moderate to high or very high, and 17.4% in areas where rock fall hazard is expected to be low or very low. The remaining 10.1% of the earthquake induced failures occurred in areas where rock falls are not forecasted by the model. The latter, are largely due to minor inconsistencies in the DEM used to perform the simulation.

Immediately after the earthquakes of September-October 1997, the Government of Umbria and the National Road Company (ANAS) invested considerable resources to install defensive measures to mitigate rock fall hazard and risk along the Nera River and the Corno River valleys. Four types of defensive measures were installed: (i) passive revetment nets, (ii) elastic rock fences, (iii) concrete retaining walls, and (iv) artificial tunnels. The remedial measurements were taken without considering the hazard assessment discussed here. Also, the rock fall hazard assessment shown in Figure 7.12 does not consider the presence of the defensive measures. Hence, the model locally overestimates the hazard and the associated risk.

To determine the mitigating effects of existing defensive structures, I now perform a set of three additional simulations. The first simulation (Model 2, Table 7.5) considers the presence of the passive revetment nets. The areas where passive revetment nets were installed were mapped in the field using the same base maps at 1:10,000 scale used to identify the rock fall source areas. A total of 0.3 km^2 of revetment nets were mapped, mostly along or in the vicinity of the roads. The revetment nets are assumed fully capable of preventing rock falls, i.e., that no boulder could detach or fall where the revetment nets are present. Based on this assumption, a new rock fall hazard model is prepared that differed from the previous model (shown in Figure 7.12) only in terms of the reduced extent of the rock fall source areas. In this new model the total rock fall source areas extend for 1.7 km^2 (Table 7.5). According to the new model, the area potentially affected by rock falls decreases to 6.5 km^2 (13.5%) and the length of roads subject to rock fall hazard decreases to 6.5 km (20.5%). The presence of the passive revetment nets reduces by 7.4% the extent of the area potentially subject to rock falls, and by about 27.9% the total length of roads subject to rock fall hazard. The reduction is larger along the roads than in the rest of the hazardous areas.

In the second simulation (Model 3, Table 7.5) the presence of the other defensive structures, namely the elastic rock fences, the concrete barriers, and the artificial tunnels, is considered. For simplicity, the possibility of a boulder that breaks through, or flies over an elastic fences or a concrete barrier is excluded. Rock fences and concrete barriers are linear features in plan view, and for modelling purposes they are transformed into strips of adjacent pixels 5 m × 5 m in size. A new rock fall hazard model is prepared taking into account the presence of the revetment nets (i.e., reducing the extent of the rock fall source area), the location of the elastic rock fall fences and concrete barriers (i.e., the rock fall retaining structures), and the presence of the artificial tunnels. The new model reveals that the extent of the area subject to rock fall

hazard decreases to 6.3 km^2 (13.1%). Correspondingly, the total length of road subject to rock fall hazard reduces to 2.9 kilometres, or 9.2% of the considered road network. The analysis indicates that the combined effect of all the existing defensive structures reduced by about 10.4% the extent of the area subject to rock falls, and by about 67.8% the total length of roads subject to rock fall hazard. Again, the reduction is larger along the roads than in other areas, because of the location of the defensive structures, which were installed chiefly along or in the immediate vicinities of the roads.

Table 7.5 – Nera River and the Corno River valleys. Comparison of different rock fall hazard models prepared considering and not considering the presence and efficacy of the rock fall defensive structures installed in the area.

		Rock Fall source area	*Affected area*		*Affected roads*	
		km^2	km^2	%	km	%
Model 1	Defensive measures not considered	2.0	7.0	14.6	9.0	28.5
Model 2	Revetment nets considered	1.7	6.5	13.5	6.5	20.5
Model 3	All defensive measures present in the area, considered fully efficient	1.7	6.3	13.1	2.9	9.2
Model 4	All defensive measures present in the area, efficacy is considered	1.7	6.4	8.9	4.1	12.8

The third simulation (Model 4, Table 7.5) consists in the evaluation the efficacy of the rock fall retaining structures. This is accomplished in two steps. First, for each grid cell the maximum height of the computed rock fall trajectories was compared to the height of the retaining structures. The analysis revealed that 20.7% of the retaining structures could be "jumped" by high flying rocks. Then, the possibility that a boulder could have enough kinetic energy to break through an elastic fence or a concrete wall was considered. For the purpose, it was assumed that the retaining structures could absorb up to 2500 kJ, a reasonable value for the structures present in the study area. At each grid cell the maximum computed rock fall velocity was used to calculate the corresponding boulder maximum kinetic energy, assuming a characteristic volume of 2 cubic meters and a unit weight of 2500 kg·m^3. The latter spatial analysis reveals that 10.2% of the existing retaining structures can be destroyed or damaged by falling blocks. The analysis also shows that 21.0% of the rock fall elastic fences or concrete walls can be either bypassed by high flying rock falls, or can be damaged or destroyed by fast moving boulders. These defensive structures are at least partly ineffective in protecting from rock falls. The final step in the analysis consists in preparing a last hazard model not considering the presence of the "ineffective" defensive structures. This last model reveals that 4.1 km of roads in the study area (12.8%) are potentially subject to rock fall hazard. The combined effect of all the effective defensive structures reducs by about 8.9% the total extent of the area subject to rock falls, and by about 55.1% the total length of roads subject to rock fall hazard. The model indicates that, despite the considerable reduction in rock falls risk due to the presence of numerous defensive structures, residual risk still exists along roads in the Nera River and the Corno River valleys.

7.5.4. Discussion

I now briefly discuss the results obtained in the assessment of rock fall hazard along the Nera River and the Corno River valleys. The discussion focuses on the performed experiment, but conclusions are applicable to other areas and, more generally, I consider them relevant to the application of process-based models for the assessment of landslide susceptibility and hazard (§ 6.2.3.5).

The model of the rock fall process implemented in the computer code STONE is necessarily simplified (Guzzetti *et al.*, 2002; Agliardi and Crosta, 2004). Constraints in the model reflect into the software outputs and in the hazard assessment. In the shown experiment, selection of the input parameters required by STONE was heuristic and to some extent arbitrary. The horizontal starting velocity was kept constant (in scale and direction) throughout the study area, and was not selected considering the ground movements measured at nearby accelerometer stations. Values of the parameters used to simulate the loss of energy where boulders are rolling and at the impact points (Table 7.4) were selected heuristically, without any field experiment (which however is difficult to perform). The version of the software STONE used for the analysis does not consider the volume, shape and mass of the falling boulder (i.e., fully kinematic modelling). The simplification may be relevant where the boulder is flying at high speeds along ballistic trajectories (air friction is neglected), and at impact points, where the shape, volume and mass of the boulder are important to determine the energy lost during impact and the velocity and direction of the flying boulder. The implemented model does not consider sliding of the boulder, which may be important in the early stages of a rock fall (i.e., in the detachment area) and at the impact point. Finally, the model does not consider the possibility that at impact points a boulder may brake and rock fragments fly in different directions at various velocities. This is a condition that exists in nature, and that can result in very hazardous situations.

The quality of the rock fall simulation depends also on other factors, including the complete and accurate identification of rock fall source cells and the quality of the DEM. Over large areas the detachment areas of rock falls are not easy to identify and map precisely. Minor rock slopes and small road cuts may not be shown in the map of the rock fall source cells. As a consequence the model may locally underestimate the spatial extent of the rock fall problem. Where terrain is very steep and bedrock crops out, contour lines were not shown in the base maps. In these areas the DEM does not accurately represent the topography, and the rock fall hazard model may be locally imprecise.

Values of the adopted rock fall hazard index do not provide an absolute ranking of hazard levels. If the extreme values are easy to define, intermediate conditions of rock fall hazard are more difficult to rank. A grid cell where rock fall frequency is very low and the flying height and velocity are very low (H_{RF} = 111) will have a much lower hazard than a grid cell that exhibits very high rock fall frequency, and very large flying height and velocity (H_{RF} = 555). Deciding whether a grid cell with very high frequency and light rock fall intensity (H_{RF} = 511) has a larger hazard than that of a grid cell with very low expected frequency and very high rock fall intensity (H_{RF} = 155) is not straightforward, and may be a matter of opinion or local judgment (e.g., Cardinali *et al*., 2002; Reichenbach *et al*., 2005).

The evaluation of the efficacy of the rock fall defensive structures is affected by completeness and resolution of the mapping. Identification of revetment nets, elastic rock fences, and rock walls was straightforward, but accurate mapping was locally difficult due to the size of the structures (locally a few tens of square meters) compared to the scale of the maps (1:10,000).

When estimating the mitigating effects of the revetment nets, the assumption was made that structures were completely efficient in preventing the detachment of rock falls. The assumption may be incorrect where large boulders are expected. The output of the computer model provided information only on the maximum values of the rock fall flying height and travel velocity. Average, or modal values were not considered and the frequency of the extreme values remains unknown. For the identification of the sections of the retaining structures that were unable to catch all the high-flying boulders or that could be destroyed by fast moving blocks, only the maximum computed values were used. As a result, the extent of the potentially ineffective retaining structures may have been overestimated. In addition, the estimate of the efficacy of the retaining structures did not consider the presence of multiple sets of elastic fences along the slopes.

As a result of these considerations, the spatial evaluation of the rock fall hazard along the Nera River valley and the assessment of the possible associated risk along the roads are undoubtedly affected by uncertainties and limitations that must be considered when using the model results for mitigation and planning purposes.

7.6. Summary of achieved results

In this chapter, I have:

(a) Proposed a probabilistic model for the assessment of landslide hazard, which fulfils a standard definition of landslide hazard.

(b) Tested the proposed model at the catchment scale, exploiting geomorphological information on slope failures obtained from a multi-temporal landslide inventory map.

(c) Demonstrated that probabilistic landslide hazard assessment can be conducted at the national scale. However, verification of the validity of the many assumptions on which the model is based was not possible at the synoptic scale.

(d) Demonstrated that the proposed probabilistic framework can also be adopted to determine the hazard posed by rock falls – a different type of mass movement – exploiting results obtained by a 3-dimensional rock fall simulation model.

This responds to Question # 6 posed in the Introduction (§ 1.2).